Tellus (1998), 50B, 290–316
Printed in UK – all rights reserved

TELLUS
ISSN 0280–6495

A latitude-depth, circulation-biogeochemical ocean model for paleoclimate studies. Development and sensitivities

By OLIVIER MARCHAL*, THOMAS F. STOCKER and FORTUNAT JOOS, *Climate and Environmental Physics, Physics Institute, 5 Sidlerstrasse, University of Bern, CH-3012 Bern, Switzerland*

(Manuscript received 2 May 1997; in final form 21 January 1998)

ABSTRACT

We extend a zonally-averaged, global ocean circulation model to include a simple description of the cycles of organic carbon and $CaCO_3$. The circulation in the model is first calibrated so that basin mean vertical profiles of temperature, salinity and radiocarbon agree closely with data for the modern oceans. Then, the capability of the model to reproduce the observed large-scale distribution of five biogeochemical tracers (phosphate, oxygen, total dissolved inorganic carbon (DIC), alkalinity (ALK) and $\delta^{13}C$ of DIC) is investigated. If organic carbon is transported only as fast-sinking particles with a remineralization profile constrained from sediment trap data, large PO_4 excesses and anoxia are simulated in subsurface waters in the equatorial Pacific and Indian Oceans. As in 3-dimensional models, these features disappear if a significant fraction (σ) of organic carbon is allowed to be exported away from production sites as labile dissolved organic carbon (DOC_l). With $\sigma = 0.5$ and an ocean mean DOC_l of 10 mmol m^{-3}, the latitude-depth distributions of PO_4 and apparent O_2 utilization in the different basins are in agreement with climatological data. The basin mean vertical profiles of DIC, ALK and $\delta^{13}C_{DIC}$ compare favourably with observations in the modern oceans. The model predicts a global new production of 6.3–10.8 GtC yr^{-1}, a rate consistent with data- and model-based estimates.

1. Introduction

High-resolution analyses of deep sea sediments suggest that the formation of North Atlantic Deep Water, a key component of the ocean thermohaline circulation and hence of climate, has changed frequently and abruptly during the last glacial period (Boyle and Keigwin, 1987; Keigwin et al., 1991; Cortijo et al., 1995; Oppo and Lehman, 1995; Maslin et al., 1995; Rasmussen et al., 1996; Vidal et al., 1997). Those changes are thought to play a prominent role in stadial-to-interstadial (Broecker et al., 1985a) and glacial-to-interglacial transitions (Broecker and Denton, 1989) and lead to significant variations in the atmospheric CO_2 content (Siegenthaler and Wenk, 1984). Box models are commonly used to investigate the geochemistry involved in changes in the thermohaline circulation: the ocean and the atmosphere are represented by well-mixed reservoirs, and exchanges between them are prescribed (Broecker and Peng, 1986, 1987; Boyle, 1988; Keir 1988, 1990). The major advantages of these models are that they are easy to formulate, and very long integrations (e.g., $\sim 10^4$ yr) are possible. This permits a rapid and first-order identification of the geochemical responses in the ocean-atmosphere system to changes in oceanic mixing rates. The main shortcoming in these models, on the other hand, is the absence of any dynamics. Alternatively, 3-dimensional ocean circulation-

* Corresponding author.
E-mail: marchal@climate.unibe.ch

biogeochemical models are used (Maier-Reimer 1993; Sarmiento et al., 1995) which are based on a much more detailed representation of the ocean circulation and superior spatial resolution. Their main disadvantage is that they remain computationally expensive so that the number of sensitivity experiments regarding the different model parameters is very limited. Another drawback of 3-d models is that they require a detailed specification of surface boundary conditions which are, especially for the glacial period, difficult to constrain.

In this paper, we fill the gap between the simple box and the complex 3-d models with a "2.5-d" ocean circulation-biogeochemical model. Here, governing equations for momentum, heat, salt and tracers are integrated from the western to the eastern boundary of each oceanic basin. Thus, the model is zonally averaged, but the Atlantic, Pacific, Indian and Southern Oceans are represented separately, with the Southern Ocean being the only connection between the individual basins. This simple structure of the marine domain is guided by a compromise between the necessity (1) to take into account the interaction between the thermohaline circulation and biological processes in governing the large-scale distribution of biogeochemical tracers in each of the major ocean basins (Broecker and Peng, 1982) and (2) to perform climatic-scale ($\sim 10^4$ yr) integrations with many sensitivity experiments. On the other hand, this structure does not permit investigation of ocean processes characterized by time scales less than a decade and by horizontal spatial scales less than several hundred to thousand kilometers. Although the model is calibrated to the modern ocean, we present a simple modification that also permits its application in paleoclimate studies. Thus, our aim is to provide a tool with which we can quantitatively study the impact of fast changes in the ocean circulation on the large-scale distribution of biogeochemical tracers in the ocean, such as $\delta^{13}C_{DIC}$ in the deep sea (Vidal et al., 1997), and on the concentration of atmospheric CO_2 (Siegenthaler and Wenk, 1984). It is a natural extension of previous efforts using the same model which have explored the effects of these changes on $\delta^{18}O$ in the deep ocean (Lehman et al., 1993), anthropogenic CO_2 (Stocker et al., 1994) or atmospheric radiocarbon (Stocker and Wright, 1996).

The paper is organized as follows. The model is described in Section 2. In Section 3, we analyse the sensitivity of the large-scale distribution of the tracers to critical biogeochemical parameters introduced into the model. Here, model results are systematically compared to observations in the modern oceans. Results are discussed in Section 4 and conclusions follow in Section 5.

2. Model description

As we focus in this paper on the capability of the model to simulate the distribution of biogeochemical tracers in the modern oceans, the chemical and isotopic composition of the atmosphere is prescribed. In future paleoclimate applications, this restriction will be relaxed.

2.1. *Circulation model*

The ocean circulation is simulated using the global ocean circulation model of Wright and Stocker (1992) (hereafter the WS model). The basin geometry and spatial grid are those of Stocker and Wright (1996) (14 vertical cells, see Table 1, and 9–14 horizontal cells, depending on the basin, with a meridional width between $7.5^\circ - 15^\circ$). In this model, the governing equations are written in spherical coordinates and include hydrostatic, Boussinesq and rigid-lid approximations. Momentum equations are balances between Coriolis forces, horizontal pressure (P) gradients and zonal wind stress. East-west P gradients that appear upon zonally averaging these equations are calculated as a function of north-south P gradients according to the closure scheme of Wright et al. (1995). Time-dependence enters via the equations for T and S, including vertical and meridional advection, diffusion and convection. The ocean circulation is driven by restoring sea surface temperatures (T) and salinities (S) to observed annual zonal averages (*restoring boundary conditions*) and by applying annual zonal averages of wind stress in each oceanic basin derived from climatological data (Han and Lee, 1983).

Vertical (K_v) and horizontal (K_h) eddy diffusivities are taken as constant. From theoretical considerations local vertical eddy diffusivities for tracers are inversely related to the density stratification of the water column (Gargett and Holloway, 1984) and microstructure measurements in the open

Table 1. *Parameters of the ocean circulation model*

K_v	vertical eddy diffusivity	2.10^{-5}	($m^2\ s^{-1}$)
K_h	horizontal eddy diffusivity	1000	($m^2\ s^{-1}$)
γ_1	velocity closure parameter	1.1	(1)
γ_2	velocity closure parameter	-0.6	(1)
τ_T	restoring time for surface temperature	50	(d)
τ_S	restoring time for surface salinity	50	(d)
	sea ice formation rate in Southern Ocean	0.05	(Sv)
	deep water formation rate in Southern Ocean	5	(Sv)
	restoring surface salinity at 72.5°N in Atlantic	35.0	(1)
Δz	bottom depths of model cells	50, 100, 150, 250, 500, 750, 1000, 1250, 1500, 2000, 2500, 3000, 3500, 4000	(m)
	ridge height in Southern Ocean	2000	(m)
ρ_*	reference density	1028	($kg\ m^{-3}$)
a	earth's radius	6371	(km)
g	earth's gravitational acceleration	9.81	($m\ s^{-2}$)

ocean indicate that local diffusivity varies with depth (Toole et al., 1994). However, in the model, the diffusivity parametrization accounts for all tracer transport which cannot be explicitly described due to the limited spatial and temporal resolution of the model. Therefore, diffusivity coefficients (K_v, K_h) applied in our coarse resolution model are not comparable to local diffusivities derived from microstructure measurements as different space and time scales are considered.

Three minor modifications to the published models are included. First, surface restoring T and S are calculated by zonally averaging in each basin the climatological data of Levitus and Boyer (1994a) and Levitus et al. (1994), respectively (excluding data from the Hudson Bay, the Baltic Sea and the Mediterranean). Second, parameter values with respect to deep water formation, i.e. the rates of sea ice and deep water formation along the Antarctic perimeter and the restoring S at 72.5°N in the Atlantic are changed (Table 1). Finally, density is computed from T, S and P using the non-linear equation of state of Wright (1996). Model results are analysed after 10 kyr of integration.

In order to assess the ventilation rate of the different basins, radiocarbon is included in the model as an inorganic tracer using the arbitrary scale of Toggweiler et al. (1989) to express the $^{14}C/^{12}C$ ratio. The decay constant of ^{14}C is $1/8267\ yr^{-1}$ and the time scale of restoring to atmospheric $\Delta^{14}C$ is 6 yr (Stocker et al., 1994). The atmospheric composition is uniformly fixed to 100 units, except for the last 175 yr of integration for which the ocean surface radiocarbon is relaxed to atmospheric $\Delta^{14}C$ observed between 1800–1975 in the extratropical southern and northern hemispheres and in the tropical belt (Fig. B.5 in Enting et al., 1994).

Fig. 1a–c compares basin mean vertical profiles of T, S, and $\Delta^{14}C$ simulated by our model with T data of Levitus and Boyer (1994a), S data of Levitus et al. (1994) and with GEOSECS (1987) $\Delta^{14}C$ data. These profiles represent volume-weighted averages in the Atlantic (between 47.5°S–80°N), Southern Ocean (between 70°S–47.5°S everywhere), Indian (47.5°S–20°N) and Pacific (47.5°S–55°N). We test the sensitivity of the different profiles to uniform K_v ranging from $10^{-5}\ m^2\ s^{-1}$ to $10^{-4}\ m^2\ s^{-1}$. This range encompasses typical estimates of the diapycnal diffusivity based on microstructure measurements and tracer balances in the open ocean (Gregg, 1987; Ledwell et al., 1993; Toole et al., 1994). The root-mean-square deviations produced by the model when using different values of K_v are calculated for each oceanic basin defined above. With $x \in \{T, S, \Delta^{14}C\}$,

$$\mathrm{rms}(x) = \sqrt{\sum_i v_i (x_i^d - x_i^s)^2 \Big/ \sum_i v_i},$$

where x_i^d is a data-derived value, x_i^s is a simulated value, and v_i is the volume of the cell centered at grid point i. Using $K_v = 10^{-4}\ m^2\ s^{-1}$ generally produces the largest errors in the predicted profiles of T, S and $\Delta^{14}C$. In this case, waters are too warm and too young at depth in each basin and

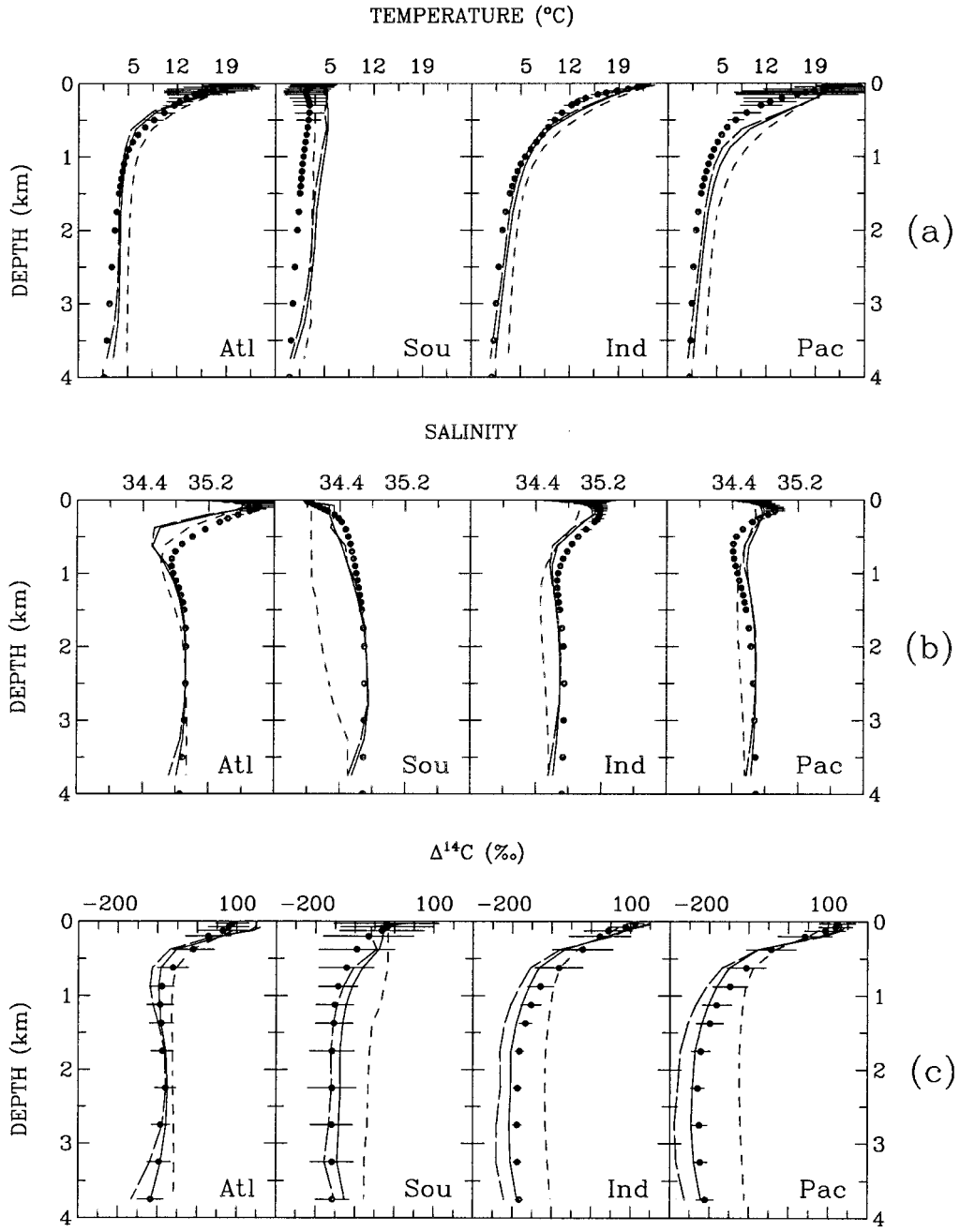

Fig. 1. Basin mean vertical profiles of (a) temperature, (b) salinity and (c) $\Delta^{14}C$ of dissolved inorganic carbon. Dots (●) are volume-weighted averages computed from the data of (a) Levitus and Boyer (1994a), (b) Levitus et al. (1994) and (c) GEOSECS (1987) interpolated onto the vertical model grid. Horizonal bars denote 1 standard deviation around these averages. The three curves are model results with $K_v = 0.1 \cdot 10^{-4}\ m^2\ s^{-1}$ (— — —), $0.2 \times 10^{-4}\ m^2\ s^{-1}$ (———) and $1.0 \cdot 10^{-4}\ m^2\ s^{-1}$ (– – –).

too fresh in the Southern Ocean (Fig. 1). Agreement improves when K_v is decreased to $1–2 \cdot 10^{-5}$ m^2 s^{-1} with rms$(T) = 1.1–2.3$°C and rms$(S) = 0.1–0.3$ (depending on the ocean basin and K_v). The basin mean vertical profiles of T and S are relatively similar in the simulations with $K_v = 1 \cdot 10^{-5}$ m^2 s^{-1} and $K_v = 2 \cdot 10^{-5}$ m^2 s^{-1}. However, significant differences in Δ^{14}C values are found at depth in each basin, reaching 45‰ in the deep Pacific. The best agreement between model and GEOSECS Δ^{14}C is obtained with $K_v = 2 \cdot 10^{-5}$ m^2 s^{-1} with rms$(\Delta^{14}C) =$ 30–42‰. Table 1 summarizes the circulation parameters adopted in this study.

The steady-state meridional overturning circulation simulated with parameters of Table 1 is qualitatively similar to that illustrated in previous studies (Stocker et al., 1994; Stocker and Wright, 1996). Here, the maximum thermohaline overturning is about 24 Sv in the North Atlantic (1 Sv $= 10^6$ m^3 s^{-1}). This value is slightly higher than, but still consistent with, the estimates of 14–20 Sv reported by Gordon (1986) and Schmitz (1995). About 16 Sv are recirculated within the Atlantic and the remaining water exits into the Southern Ocean south of 47.5°S. From there, this water enters the other basins via the circumpolar current. Broad upwelling then occurs in the deep Pacific and deep Indian.

2.2. Biogeochemical model

2.2.1. Tracers. The biogeochemical processes to be taken into account in the model are the cycling of organic matter and carbonate particles (Volk and Hoffert, 1985). We treat these processes largely on the basis of previous 3-d circulation-biogeochemical models (Sections 2.2.2–2.2.5). For instance, the new production, i.e. the primary production supported by nutrient fluxes from outside the euphotic zone (Dugdale and Goering, 1967), is assumed to lead to a net export of organic matter from the euphotic zone (no net accumulation of organic matter). Also, river input or sediment burial are not included, i.e. all the organic matter and $CaCO_3$ are recycled in the water column (Najjar et al., 1992; Sarmiento et al., 1995; Yamanaka and Tajika, 1996).

The biogeochemical tracers transported explicitly by the circulation are phosphate (PO_4), oxygen (O_2), total dissolved inorganic carbon (DIC), alkalinity (ALK), labile dissolved organic carbon (DOC_l), ^{13}C in DIC ($DI^{13}C$) and ^{13}C in DOC_l ($DO^{13}C_l$). The following continuity equation is solved for each of these tracers ($\mathscr{T}$):

$$\frac{\partial \mathscr{T}}{\partial t} + \frac{1}{a \cos\phi} \frac{\partial}{\partial \phi} (\cos\phi v \mathscr{T}) + \frac{\partial}{\partial z}\left(w\mathscr{T}\right) = \frac{1}{a^2 \cos\phi} \frac{\partial}{\partial \phi}\left(K_h \cos\phi \frac{\partial \mathscr{T}}{\partial \phi}\right) + \frac{\partial}{\partial z}\left(K_v \frac{\partial \mathscr{T}}{\partial z}\right) + q^{\mathscr{T}}_{conv} + (J^{\mathscr{T}}_{org} + J^{\mathscr{T}}_{car}), \quad (1)$$

where t is time, z is the depth (positive z upward), ϕ is latitude, a is earth's radius, v and w are the meridional and vertical components of velocity, K_h and K_v are the horizontal and vertical eddy diffusivities (both constant), $q^{\mathscr{T}}_{conv}$ denotes convection, and $J^{\mathscr{T}}_{org}$ and $J^{\mathscr{T}}_{car}$ are the source minus sink terms associated with the cycling of organic matter and carbonate particles, respectively. All quantities in eq. (1) are zonal averages. In deriving this equation, it is assumed that the meridional transport associated with the correlation between the wind-driven gyre circulation and the east-west tracer difference is negligible compared to the transport associated with the thermohaline circulation (Wright and Stocker, 1992).

Phosphate is taken here as the nutrient limiting the biological productivity (Najjar et al., 1992; Maier-Reimer, 1993; Yamanaka and Tajika, 1996). Whether this role is played by phosphate or nitrate in the real ocean is actually debated (Smith, 1984; Hecky and Kilham, 1988; Codispoti, 1989; Falkowski, 1997). Using phosphate has the advantage that the processes of N_2 fixation and denitrification need not be formulated, and a well-documented data set is available (Conkright et al., 1994; Tyrrell and Law, 1997). Oxygen, on the other hand, is included as a test of the oxidation of organic matter. The apparent O_2 utilization (AOU) is calculated from O_2 and the saturation level using the formula of Weiss (1970) and assuming an atmospheric partial pressure of $O_2 = 0.2095$ atm (Machta and Hughes, 1970). Finally, the isotopic composition of DIC ($= DI^{12}C + DI^{13}C$) is referenced to the PDB standard, i.e. $\delta^{13}C_{DIC} = (r/r_{std} - 1) \times 1000$, where $r = DI^{13}C/DI^{12}C$ and $r_{std} = 0.0112372$ (Craig, 1957).

A paradigm identifies the sinking of particulate organic carbon (POC) as the dominant export of reduced C from the ocean euphotic zone (Brewer

and Glover, 1987). Although both the inventory (Martin and Fitzwater, 1992) and biological lability of marine dissolved organic C (DOC) (Bauer et al., 1992; Amon and Benner, 1994) remain controversial, field data highlight the additional role of DOC in this export. Indeed, DOC measurements in contrasting marine environments indicate that the downward flux of DOC from the euphotic zone compete with the flux of fast-sinking particulate organic C (POC) as caught in sediment traps (Copin-Montégut and Avril, 1993; Carlson et al., 1994; Murray et al., 1994; Guo et al., 1995; Ducklow et al., 1995). In their 3-d ocean circulation–biogeochemical models, Bacastow and Maier-Reiner (1991) and Najjar et al. (1992) first considered organic matter only in the form of fast-sinking particulate organic matter (POM) that remineralize at depth according to a profile consistent with sediment trap data. These models produce subsurface PO_4 excesses in equatorial areas relative to observations. This nutrient trapping was ascribed to a positive feedback peculiar to equatorial circulation regimes, whereby upwelling of nutrients increases new production, remineralization at depth and the nutrient content of the upwelling water (Najjar et al., 1992). It is removed if a substantial fraction (70–80%) of the organic matter is in dissolved phase (Bacastow and Maier-Reimer, 1991; Najjar et al., 1992). Matear and Holloway (1995), on the other hand, showed that failures of a 3-d model to reproduce the observed PO_4 distribution in the North Pacific disappear to a large extent if only small changes are introduced in the circulation field.

Here, following Bacastow and Maier-Reimer (1991), Najjar et al. (1992) and Yamanaka and Tajika (1997), we compare model results produced when organic carbon is either only in the form of settling POC or in the form of both settling POC and labile dissolved organic carbon, DOC_l. The potential for the ocean circulation simulated by our model to produce deficiencies in the nutrient distribution is discussed in Section 4. When DOC_l is included in the model, ^{13}C in labile $DO^{13}C_l$ ($DO^{13}C_l$) is also simulated so that the amount of inorganic ^{13}C reduced into DOC_l in the euphotic zone is balanced by the amount of inorganic ^{13}C produced by DOC_l oxidation at depth. Unlike DOC_l and $DO^{13}C_l$, the fast-sinking POC is not transported explicitly by the circulation, for it is remineralized below the euphotic zone as soon as it is produced.

In the model, each tracer is defined as a salinity-normalized concentration (in $\mathrm{mmol\,m^{-3}}$), i.e. $\mathscr{T} = \mathscr{T}_a \cdot \bar{S}/S$, where $\mathscr{T}_a$ is the actual concentration and $\bar{S} = 34.73$ is the modern ocean mean salinity (Levitus et al., 1994). Normalization to salinity avoids the need for an explicit formulation of the effect of surface freshwater fluxes in the continuity eq. (1).

2.2.2. Biogeochemical processes in the euphotic zone ($z < z_{eup}$). In order to obtain well-defined tracer fields, the concentrations of PO_4 in the euphotic zone (top 100 m) are directly restored to the observations in the modern oceans, PO_4^r, if PO_4 in the model $> PO_4^r$ (Najjar et al., 1992). A single value of PO_4^r is determined at each cell of the model grid by zonally- and depth-averaging the climatological data of Conkright et al. (1994) (Fig. 2). The change in tracer due to new production ($J^{\mathscr{T}}_{org}$) and $CaCO_3$ production ($J^{\mathscr{T}}_{car}$) in the euphotic zone are then parameterized as:

$$J^{\mathscr{T}}_{org} = r^{\mathscr{T}}_{org} \frac{PO_4^r - PO_4}{\tau_{PO_4}} \quad (J^{\mathscr{T}}_{org} = 0 \text{ for } PO_4 \leqslant PO_4^r), \tag{2}$$

$$J^{\mathscr{T}}_{car} = r^{\mathscr{T}}_{car} r_p J^{DIC}_{org}. \tag{3}$$

τ_{PO_4} is a restoring time scale. $r^{\mathscr{T}}_{org}$ are Redfield atomic ratios, referenced to P, for the formation of organic matter (e.g., $r^{DIC}_{org} \equiv C:P$) and $r^{\mathscr{T}}_{car}$ are the atomic ratios, referenced to C, for the formation of $CaCO_3$ (e.g., $r^{DIC}_{car} = 1$). r_p is the production ratio, i.e., the ratio between the production of $CaCO_3$ to the production of organic C ($POC + DOC_l$) in the euphotic zone. This ratio is different from the so-called "rain ratio" to the extent that DOC_l makes up a portion of the organic C. The rationale for using (2) is that the ocean circulation in the model tends to "push" PO_4 in the euphotic zone above PO_4^r due to the upwelling of deep nutrient-rich waters. This permits diagnosis of rates of new production ($J^{\mathscr{T}}_{org}$) that are consistent with the observed nutrient distributions in each oceanic basin (Najjar et al., 1992). We show in Section 4.3 how these rates can be used to calibrate a prognostic description of the biological activity.

As a working hypothesis, $r^{\mathscr{T}}_{org}$ and $r^{\mathscr{T}}_{car}$ are taken constant with time and location (except for $r^{O_2}_{org}$ in

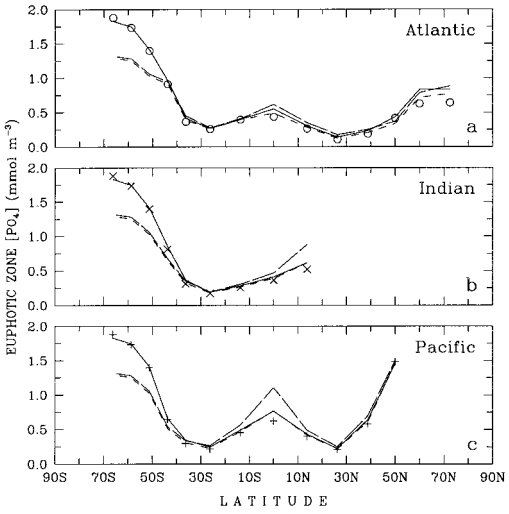

Fig. 2. Annual zonal mean concentration of phosphate in the top 100 m in the three main ocean basins. Symbols are observed restoring values PO_4^r. Results from the POC-only model with $\tau_{PO_4} = 200$ d (— — —), 50 d (– – –) and from the $POC + DOC_l$ model with $\tau_{PO_4} = 100$ d (———) are shown. Concentrations are normalized to the ocean mean salinity of 34.73.

the euphotic zone; Subsection 2.2.5). From mean remineralization ratios in the deep sea determined by Anderson and Sarmiento (1994), we adopt the following ratios for the cycling of organic matter:

$$r_{org}^{PO_4} = 1, \tag{4}$$

$$r_{org}^{DIC} = 117, \tag{5}$$

$$r_{org}^{ALK} = -16, \tag{6}$$

$$r_{org}^{DOC_l} = -117\sigma, \tag{7}$$

$$r_{org}^{DI^{13}C} = 117\alpha_{org}\frac{DI^{13}C}{DIC}, \tag{8}$$

$$r_{org}^{DO^{13}C_l} = -117\alpha_{org}\frac{DI^{13}C}{DIC}\sigma, \tag{9}$$

where σ is the fraction of reduced C sequested into DOC_l and α_{org} is the fractionation factor for photosynthesis. For $CaCO_3$ formation, we take:

$$r_{car}^{PO_4} = r_{car}^{DOC_l} = r_{car}^{O_2} = r_{car}^{DO^{13}C_l} = 0, \tag{10}$$

$$r_{car}^{DIC} = 1, \tag{11}$$

$$r_{car}^{ALK} = 2, \tag{12}$$

$$r_{car}^{DI^{13}C} = \alpha_{car}\frac{DI^{13}C}{DIC}, \tag{13}$$

where α_{car} is the fractionation factor for calcification.

Finally, we need to specify the production ratio r_p. There is an indication from sediment trap data that the contribution of the carbonate particle flux in the total particle flux is relatively low in the polar oceans (Honjo, 1990). Heinze (1990) and Drange (1994) took this into account in their 3-d circulation-biogeochemical model by expressing the production ratio (more precisely, the rain ratio in their case) as a function of temperature:

$$r_p = r_{p,m}\frac{p_1\, e^{p_2(T-T_r)}}{1 + p_1\, e^{p_2(T-T_r)}}, \tag{14}$$

where T_r is a reference temperature, $r_{p,m}$ is the maximum value of the production ratio that would occur in warm waters (i.e. for $T \gg T_r$) and p_1, p_2 are parameters. We include eq. (14) in our model with $T_r = 10°C$, $p_1 = 1$ and $p_2 = 0.6°C^{-1}$ (Drange, 1994). Averaging (14) with these values in the range of sea surface temperature from -2 to 30°C, the maximum production ratio in the model is related to the ocean mean production ratio, $\overline{r_p}$, by $r_{p,m} = 1.6\overline{r_p}$.

2.2.3. Biogeochemical processes in the aphotic zone ($z > z_{eup}$). The remineralization of organic C and the redissolution of $CaCO_3$ are assumed to take place only in the aphotic zone. Organic C in the model is in the form of both fast-sinking POC and DOC_l (see above). Following Najjar et al. (1992), the fast-sinking POC is immediately remineralized according to a power-law with exponent ε as determined from sediment trap data (Martin et al., 1987, 1993; Bishop, 1989). We take $\varepsilon = 0.858$, producing the best fit to sediment trap data among eight different empirical relationships describing the particle flux in the open ocean (Bishop, 1989). The oxidation of DOC_l is assumed to follow first-order kinetics with a rate constant κ. Other potentially influencing factors such as depth-changes in the biomass of heterotrophic bacteria (major DOC consumers), temperature or pressure, are neglected here (Bacastow and Maier-Reimer, 1991; Najjar et al., 1992). Finally, dissolution of $CaCO_3$ is assumed to vary with depth according to an exponential profile with a length scale L_{dis} (Maier-Reimer, 1993; Yamanaka and Tajika, 1996).

With $J_{pom}^{\mathscr{F}}$ and $J_{dom}^{\mathscr{F}}$, respectively the local rates of remineralization associated with the recycling

of fast-sinking POM and with dissolved organic matter, DOM,

$$J^{\mathscr{T}}_{\mathrm{org}} = J^{\mathscr{T}}_{\mathrm{pom}} + J^{\mathscr{T}}_{\mathrm{dom}} = -\frac{\partial F^{\mathscr{T}}_{\mathrm{pom}}}{\partial z} + \kappa^{\mathscr{T}}\,\mathrm{DOC}_l, \quad (15)$$

$$J^{\mathscr{T}}_{\mathrm{car}} = -\frac{\partial F^{\mathscr{T}}_{\mathrm{car}}}{\partial z}, \quad (16)$$

where $F^{\mathscr{T}}_{\mathrm{pom}}$ and $F^{\mathscr{T}}_{\mathrm{car}}$ are the fluxes of the specific tracer associated with fast-sinking POM and carbonate particles at a given depth in the water column, and $\kappa^{\mathscr{T}}$ is the decay rate of DOC_l associated with the specific tracer $\mathscr{T}$. $F^{\mathscr{T}}_{\mathrm{pom}}$ and $F^{\mathscr{T}}_{\mathrm{car}}$ are related to the fluxes of fast-sinking POM and $CaCO_3$ at the base of the euphotic zone, $F^{\mathscr{T}}_{\mathrm{pom}}(z_{\mathrm{eup}})$ and $F^{\mathscr{T}}_{\mathrm{car}}(z_{\mathrm{eup}})$:

$$F^{\mathscr{T}}_{\mathrm{pom}}(z) = F^{\mathscr{T}}_{\mathrm{pom}}(z_{\mathrm{eup}})\left(\frac{z}{z_{\mathrm{eup}}}\right)^{-\varepsilon} = (1-\sigma)\int_0^{z_{\mathrm{eup}}} J^{\mathscr{T}}_{\mathrm{org}}\,\mathrm{d}z\left(\frac{z}{z_{\mathrm{eup}}}\right)^{-\varepsilon}, \quad (17)$$

$$F^{\mathscr{T}}_{\mathrm{car}}(z) = F^{\mathscr{T}}_{\mathrm{car}}(z_{\mathrm{eup}})(\mathrm{e}^{-(z-z_{\mathrm{eup}})/L_{\mathrm{dis}}}) = \int_0^{z_{\mathrm{eup}}} J^{\mathscr{T}}_{\mathrm{car}}\,\mathrm{d}z(\mathrm{e}^{-(z-z_{\mathrm{eup}})/L_{\mathrm{dis}}}), \quad (18)$$

where $F^{\mathrm{DOC}_l}_{\mathrm{pom}}(z) = F^{\mathrm{DO}^{13}\mathrm{C}_l}_{\mathrm{pom}}(z) = 0$. $\kappa^{\mathscr{T}}$, on the other hand, is calculated from the stoichiometry of Anderson and Sarmiento (1994):

$$\kappa^{\mathrm{PO_4}} = \frac{\kappa}{117}, \quad (19)$$

$$\kappa^{\mathrm{DIC}} = \kappa, \quad (20)$$

$$\kappa^{\mathrm{ALK}} = \frac{-16}{117}\kappa, \quad (21)$$

$$\kappa^{\mathrm{DOC}_l} = -\kappa, \quad (22)$$

$$\kappa^{\mathrm{O_2}} = \frac{-170}{117}\kappa, \quad (23)$$

$$\kappa^{\mathrm{DI}^{13}\mathrm{C}} = R_{\mathrm{DOC}_l}\kappa, \quad (24)$$

$$\kappa^{\mathrm{DO}^{13}\mathrm{C}_l} = -R_{\mathrm{DOC}_l}\kappa, \quad (25)$$

where R_{DOC_l} is the $^{13}\mathrm{C}/(^{12}\mathrm{C}+{}^{13}\mathrm{C})$ ratio of DOC_l ($R_{\mathrm{DOC}_l} = \mathrm{DO}^{13}\mathrm{C}_l/\mathrm{DOC}_l$). The recycling of the particles that reach the ocean floor and the calculation of κ are described in Subsection 2.2.5.

2.2.4. Gas exchanges. At the sea surface, a zero-flux condition is prescribed for PO_4, ALK, DOC_l and $\mathrm{DO}^{13}\mathrm{C}_l$. The surface concentrations of O_2 are assumed to be in dissolution equilibrium with the atmospheric O_2. This assumption is justified by the fact that the equilibration time of the ocean mixed layer for chemically inert gases ($\approx$1 month; Broecker and Peng, 1974) is comparable to the time step of resolution in our model ($\Delta t = 20$ days). Thus, surface values of AOU are equal to zero everywhere in the model domain, reasonably consistent with data for the modern oceans (Levitus and Boyer, 1994b).

Due to the much longer equilibration for CO_2 and $^{13}CO_2$ in the ocean mixed layer (Broecker and Peng, 1974), the surface exchanges of CO_2 and $^{13}CO_2$ are formulated explicitly. The net fluxes of $^{12}CO_2 + {}^{13}CO_2$ and $^{13}CO_2$ out of the ocean are given by (Siegenthaler and Münnich, 1981):

$$F^{\mathrm{C}}_{\mathrm{wa,n}} = F^{\mathrm{C}}_{\mathrm{wa}} - F^{\mathrm{C}}_{\mathrm{aw}} = \mu\,\mathrm{pCO}^{\mathrm{w}}_2 - \mu\,\mathrm{pCO}^{\mathrm{a}}_2, \quad (26)$$

$$F^{^{13}\mathrm{C}}_{\mathrm{wa,n}} = R_{\mathrm{w}}\alpha_{\mathrm{wa}}F^{\mathrm{C}}_{\mathrm{wa}} - R_{\mathrm{a}}\alpha_{\mathrm{aw}}F^{\mathrm{C}}_{\mathrm{aw}}. \quad (27)$$

$F^{\mathrm{C}}_{\mathrm{wa}}$ and $F^{\mathrm{C}}_{\mathrm{aw}}$ are the gross fluxes of CO_2 from the ocean to the atmosphere and from the atmosphere to the ocean, respectively. μ is a transfer coefficient for CO_2 at the air-sea interface. $\mathrm{pCO}^{\mathrm{w}}_2$ and $\mathrm{pCO}^{\mathrm{a}}_2$ are the partial pressures of CO_2 in the surface water and in the atmosphere, respectively. $\mathrm{pCO}^{\mathrm{w}}_2$ is calculated from surface T, S, DIC and ALK, assuming HCO^-_3, CO^{2-}_3 and $B(OH)^-_4$ as the unique contributors to alkalinity (Skirrow, 1975). To this end, a cubic equation for the proton activity is solved analytically (Millero, 1979) using the equilibrium constants and the proportionality factor between total boron and salinity in seawater recommended by Millero (1995). R_{w} and R_{a} are the $^{13}\mathrm{C}/(^{12}\mathrm{C}+{}^{13}\mathrm{C})$ ratios of surface DIC ($R_{\mathrm{w}} = \mathrm{DI}^{13}\mathrm{C}/\mathrm{DIC}$) and atmospheric CO_2, respectively. Finally, α_{aw} and α_{wa} are the fractionation factors for the air-sea exchange of $^{13}CO_2$. In this paper, $\mathrm{pCO}^{\mathrm{a}}_2$ and R_{a} are prescribed (Subsection 3.2).

Fractionation factors for the air-sea exchange of $^{13}CO_2$ are computed from Siegenthaler and Münnich (1981) according to:

$$\alpha_{\mathrm{aw}} = \alpha_{\mathrm{k}}\alpha_{\mathrm{aq-g}}, \quad (28)$$

$$\alpha_{\mathrm{wa}} = \alpha_{\mathrm{k}}\alpha_{\mathrm{aq-DIC}}, \quad (29)$$

where α_{k} is the kinetic fractionation factor for CO_2 gas transfer across the air-sea interface, and $\alpha_{\mathrm{aq-g}}$ and $\alpha_{\mathrm{aq-DIC}}$ are the equilibrium fractionation factors between aqueous CO_2 and gaseous CO_2, and aqueous CO_2 and total dissolved inorganic carbon, respectively. These three factors are

taken from relationships established from laboratory data (Zhang et al., 1995). $\alpha_k = 0.99912$, the mean between measurements carried out at 5°C and 21°C. α_{aq-g}, on the other hand, is as an increasing function of the sea surface temperature:

$$\alpha_{aq-g} = 0.99869 + (4.9 \cdot 10^{-6}\ ^\circ\mathrm{C}^{-1})T. \quad (30)$$

Finally, α_{aq-DIC} depends on the fractionation between aqueous CO_2 and the different inorganic C species, and on DIC speciation in seawater (Siegenthaler and Münnich, 1981):

$$\alpha_{aq-DIC} = \sum_i f_i \alpha_{aq-i}. \quad (31)$$

The ionization fractions $f_{CO_2} = CO_2(aq)/DIC$, $f_{HCO_3^-} = HCO_3^-/DIC$ and $f_{CO_3^{2-}} = CO_3^{2-}/DIC$ are obtained from the calculation of pCO_2^w from ambient T, S, DIC and ALK (see above). Zhang et al. (1995) measured the isotopic fractionation of ionic C species with respect to gaseous, and not aqueous CO_2. Hence, we compute the fractionations between aqueous CO_2 and bicarbonate ions ($\alpha_{aq-HCO_3^-}$) and between aqueous CO_2 and carbonate ions ($\alpha_{aq-CO_3^{2-}}$) through the following equations:

$$\alpha_{aq-HCO_3^-} = \frac{\alpha_{aq-g}}{\alpha_{HCO_3^- - g}} = \frac{0.99869 + (4.9 \cdot 10^{-6}\ ^\circ\mathrm{C}^{-1})T}{1.01078 - (114 \cdot 10^{-6}\ ^\circ\mathrm{C}^{-1})T}, \quad (32)$$

$$\alpha_{aq-CO_3^{2-}} = \frac{\alpha_{aq-g}}{\alpha_{CO_3^{2-} - g}} = \frac{0.99869 + (4.9 \cdot 10^{-6}\ ^\circ\mathrm{C}^{-1})T}{1.00722 - (52 \cdot 10^{-6}\ ^\circ\mathrm{C}^{-1})T}. \quad (33)$$

2.2.5. Chemical balances. The ocean inventories of phosphate, alkalinity and labile dissolved organic carbon are conserved quantities in the model. The condition for constant inventories of PO_4 and ALK is satisfied by recycling in the deepest model cells the fast-sinking POC and $CaCO_3$ particles reaching the ocean floor (at depth z_{bot}). For those cells (with a thickness Δz_{bot}), POM remineralization and $CaCO_3$ dissolution are thus given by:

$$J^{\mathscr{F}}_{pom} = \frac{1}{\Delta z_{bot}} \left(\frac{z_{bot} - \Delta z_{bot}}{z_{eup}} \right)^{-\varepsilon} F^{\mathscr{F}}_{pom}(z_{eup}), \quad (34)$$

$$J^{\mathscr{F}}_{car} = \frac{1}{\Delta z_{bot}} (e^{-(z_{bot} - \Delta z_{bot} - z_{eup})/L_{dis}}) F^{\mathscr{F}}_{car}(z_{eup}). \quad (35)$$

With $\varepsilon = 0.858$, the flux of fast-sinking POC that reaches the ocean floor amounts to 4% in our model. Unlike ε which is kept fixed, we test different values for the $CaCO_3$ dissolution length, L_{dis}, because a direct observational constraint is not available. With L_{dis} ranging between 2000–4000 m (see below), the flux of $CaCO_3$ at the ocean floor varies between 14 and 38%.

The condition for a constant oceanic inventory of DOC_l requires a further constraint because DOC_l is assumed to decay with first-order kinetics. This condition is satisfied by computing κ so that the new production of DOC_l in the euphotic zone balances its decay in the aphotic zone (Najjar et al., 1992):

$$\int_A \int_0^{z_{eup}} J^{DOC_l}_{org}\, dz\, dA = \kappa \int_A \int_{z_{eup}}^{z_{bot}} DOC_l\, dz\, dA, \quad (36)$$

where A is the total ocean area. Following Najjar et al. (1992), we use eq. (36) given the lack of experimental data about the production and breakdown of marine DOC_l.

A last constraint is introduced in the oceanic budget of oxygen. The local rate of organic matter oxidation in the deep sea is crudely described in the model, for it depends only on the rate of new production in the overlying euphotic zone (Najjar et al., 1992). Consequently, this model may simulate very low (or even negative) O_2 concentrations in some regions of the water column such as below the highly productive equatorial upwellings. In those regions in the real ocean, chemical species other than dissolved O_2 (such as NO_3^-) are likely to serve as electron acceptors for respiration when O_2 is very low (Gruber and Sarmiento, 1997; Tyrrell and Law, 1997). In order to account for this, we set the local rate of O_2 consumption ($J^{O_2}_{org}$) in the aphotic zone equal to zero if the local concentration of oxygen falls below zero which is equivalent to a source of oxygen. The balance between the production of photosynthetic O_2 in surface waters and the respiratory consumption of O_2 at depth can be re-established by an appropriate determination of the stoichiometric ratio $r^{O_2}_{org}$ in the euphotic zone. Following Anderson and Sarmiento (1995), this ratio is calculated as:

$$r^{O_2}_{org} = -\frac{\int_A \int_{z_{eup}}^{z_{bot}} J^{O_2}_{org}\, dz\, dA}{\int_A \int_0^{z_{eup}} J^{PO_4}_{org}\, dz\, dA}. \quad (37)$$

Both κ and $r_{org}^{O_2}$ in the euphotic zone are calculated at each time step (eqs. (36)–(37)). In the aphotic zone, $r_{org}^{O_2}$ is kept constant and equal to the mean O_2 : P remineralization ratio determined by Anderson and Sarmiento (1994):

$$r_{org}^{O_2} = -170 \quad \text{for} \quad z > z_{eup}. \tag{38}$$

In summary, in addition to the stoichiometric ratios, the biogeochemical model described above includes 11 parameters (Table 2). In this paper, we investigate the effects of variable τ_{PO_4}, σ, $\overline{DOC_l}$, $\overline{r_p}$, L_{dis}, α_{org} and μ. The other biogeochemical parameters are always kept fixed to their values in Table 2.

3. Results

3.1. Simulation of phosphate and oxygen

In the model, PO_4 is only affected by organic matter cycling, whereas AOU is affected by organic matter cycling and dissolution equilibrium with atmospheric O_2. We explore the effect on the PO_4 and AOU distributions of the fraction of organic C sequestred into labile dissolved organic carbon, σ, and of the ocean mean concentration of labile dissolved organic carbon, $\overline{DOC_l}$. In all simulations, initial PO_4 correspond to a uniform field of 2.07 mmol m^{-3}, the ocean mean PO_4 according to climatological data (Conkright et al., 1994). The restoring time scale τ_{PO_4}, on the other hand, needs also be specified. Fig. 2 shows latitudinal distributions of euphotic zone PO_4 simulated with two distinct values of $\tau_{PO_4} = 50$ and 200 d. In each case, organic matter occurs only in the form of fast-sinking particles, i.e. $\sigma = 0$. With $\tau_{PO_4} = 200$ d, the model PO_4 is significantly lower than PO_4^r in the Southern Ocean and larger than PO_4^r in the equatorial Pacific and Indian. With a smaller $\tau_{PO_4} = 50$ d, on the other hand, the fit is largely improved in the equatorial Pacific and Indian, but not in the Southern Ocean. Taking a value as low as 25 d does not improve the fit in the Southern Ocean. As shown below, the discrepancy in the Southern Ocean can be largely corrected by allowing some fraction of organic carbon to be transported as DOC_l, i.e., with $\sigma > 0$. In all the simulations that follow, τ_{PO_4} is fixed to an intermediate value of 100 d. With this value, the euphotic zone PO_4 predicted in the northern North Atlantic is lower than with $\tau_{PO_4} = 200$ d, but higher than with $\tau_{PO_4} = 50$ d. This value of 100 d is adopted, however, because it reduces the large values of new production in the northern North Atlantic which are persistent in the model (Fig. 6a). This brings the model into better agreement with the distribution of the annual mean

Table 2. *Parameters of the ocean biogeochemical model*

				Refs.
τ_{PO_4}	restoring time for PO_4 in euphotic zone	100	(d)	
σ	fraction of reduced C in DOC_l	0.5	(1)	
$\overline{DOC_l}$	ocean mean content of DOC_l	10	(mmol m^{-3})	
$\overline{r_p}$	ocean mean production ratio	0.06	(mol mol^{-1})	
L_{dis}	length scale for $CaCO_3$ dissolution	3000	(m)	
α_{org}	fractionation factor for photosynthesis	*variable*	(1)	Rau et al. (1989)
μ	air-sea CO_2 transfer coefficient	67	(mmol m^{-2} yr^{-1} μatm^{-1})	Broecker et al. (1985b)
ε	exponent in fast-sinking POC remineralization profile[a)]	0.858	(1)	Bishop (1989)
κ	decay rate of DOC_l[a)]	*variable*	(yr^{-1})	Najjar et al. (1992)
α_{car}	fractionation factor for calcification[a)]	1	(1)	Mook (1986)
z_{eup}	depth of the euphotic zone[a)]	100	(m)	

[a)] No sensitivity analysis on this parameter in this study.

new production estimated in this basin (Campbell and Aarup, 1992).

3.1.1. Fraction of organic C in DOC_l. The oceanic inventory of DOC and of its biologically labile fraction remain largely uncertain. For example, estimates of the oceanic inventory of DOC reported by Martin and Fitzwater (1992) range by more than a factor of two. Bacastow and Maier-Reimer (1991) took an ocean average $\overline{DOC_l} \approx 20$ mmol m^{-3}, which may be too large (Suzuki, 1993). In this section, $\overline{DOC_l}$ is fixed to 10 mmol m^{-3}. Given the current uncertainty in the inventory and biological lability of marine DOC, we investigate in the next section the sensitivity of our results on $\overline{DOC_l}$.

The impact of DOC_l in the model is best demonstrated by considering the latitude-depth distributions of the different biogeochemical tracers and by calculating root mean square errors relative to observations. Fig. 3a illustrates the latitude-depth distributions of PO_4 simulated by the POC-only model ($\sigma = 0$). Although some of the observed features (Fig. 3c) are reproduced, large differences are found. A pronounced nutrient trapping is simulated at subsurface levels in the tropical Pacific and Indian. Following Bacastow and Maier-Reimer (1991), Najjar et al. (1992) and Yamanaka and Tajiko (1997), we try to remove this nutrient trapping by allowing some fraction of the organic carbon to be transported as DOC_l. We assume that half of organic C is sequestred into DOC_l ($\sigma = 0.5$) which is within the large range of estimates that can be inferred from various field studies (Table 1.2 in Najjar et al., 1992; Copin-Montégut and Avril, 1993; Carlson et al., 1994; Guo et al., 1995; Ducklow et al., 1995). PO_4 concentrations in the equatorial Pacific and Indian are now reduced significantly which brings the simulated PO_4 distributions into much closer agreement with the data (Fig. 3b). In the Atlantic, on the other hand, inclusion of DOC_l leads to higher PO_4 concentrations and has a smaller impact than in the other basins. Finally, the discrepancy in surface PO_4 in the Southern Ocean produced with the POC-only model is absent in the POC + DOC_l model (Fig. 2).

With regard to oxygen, anoxia is largely present in the North Indian between 200–1000 m and unrealistically low O_2 are predicted at depth in the whole North Pacific in the POC-only model (not shown). AOU is too high in these regions (compare Fig. 4a with Fig. 4c) suggesting excess of remineralization as the likely cause of these failures. When DOC_l is included, this is largely corrected and the O_2 and AOU distributions are in much closer agreement with the data (Fig. 4b for AOU). This requires that the rate of O_2 consumption is set to zero if $O_2 = 0$ mmol m^{-3}, because in the absence of this constraint anoxia and even negative O_2 are simulated by the POC + DOC_l model in subsurface waters in the North Indian and equatorial Pacific (not shown). As for PO_4, inclusion of DOC_l leads to higher values of the AOU in the Atlantic.

Root-mean-square deviations of PO_4 and AOU produced by the POC-only and POC + DOC_l models compared to the climatological data provide a quantitative estimate of the improvement. With $\overline{DOC_l} = 10$ mmol m^{-3}, a significant decrease of rms(PO_4) and rms(AOU), depending on σ, is obtained relative to the POC-only model (Fig. 5). The exception to this is the Atlantic, where some values of σ even lead to a worse simulation of PO_4 and AOU. Taking $\sigma = 0.5$ lowers rms(PO_4) by a factor of 2 in the Pacific, the Indian and in the Southern Ocean. By contrast, the deviation for the Atlantic is only slightly reduced (this slight reduction is due to the higher PO_4 concentrations which decrease rms(PO_4) in the South Atlantic but increases rms(PO_4) in the North Atlantic). A substantial reduction in rms (AOU) is also present in the Pacific, the Indian and in the Southern Ocean with $\sigma = 0.5$ (Fig. 5b). It is higher, however, in the Atlantic (increase of $\approx 30\%$). For the world ocean, $\sigma = 0.5$ reduces the model-data discrepancy in the PO_4 (AOU) distribution by about 45% (35%). From Figs. 3 and 4 we infer that the decrease of rms(PO_4) and rms(AOU) in the Pacific and Indian is largely due to the removal of nutrient trapping simulated by the POC + DOC_l model in the equatorial regions. The higher PO_4 and AOU levels in the Atlantic, on the other hand, are related to the oxidation of DOC_l which is largely produced in the northern North Atlantic (see below) and thence transported to depth with newly-formed deep waters.

The meridional distributions of new production simulated by the POC-only and POC + DOC_l models with $\sigma = 0.5$ and $\overline{DOC_l} = 10$ mmol m^{-3} are given in Fig. 6a–c. New production in the equatorial Pacific and Indian decreases by a factor

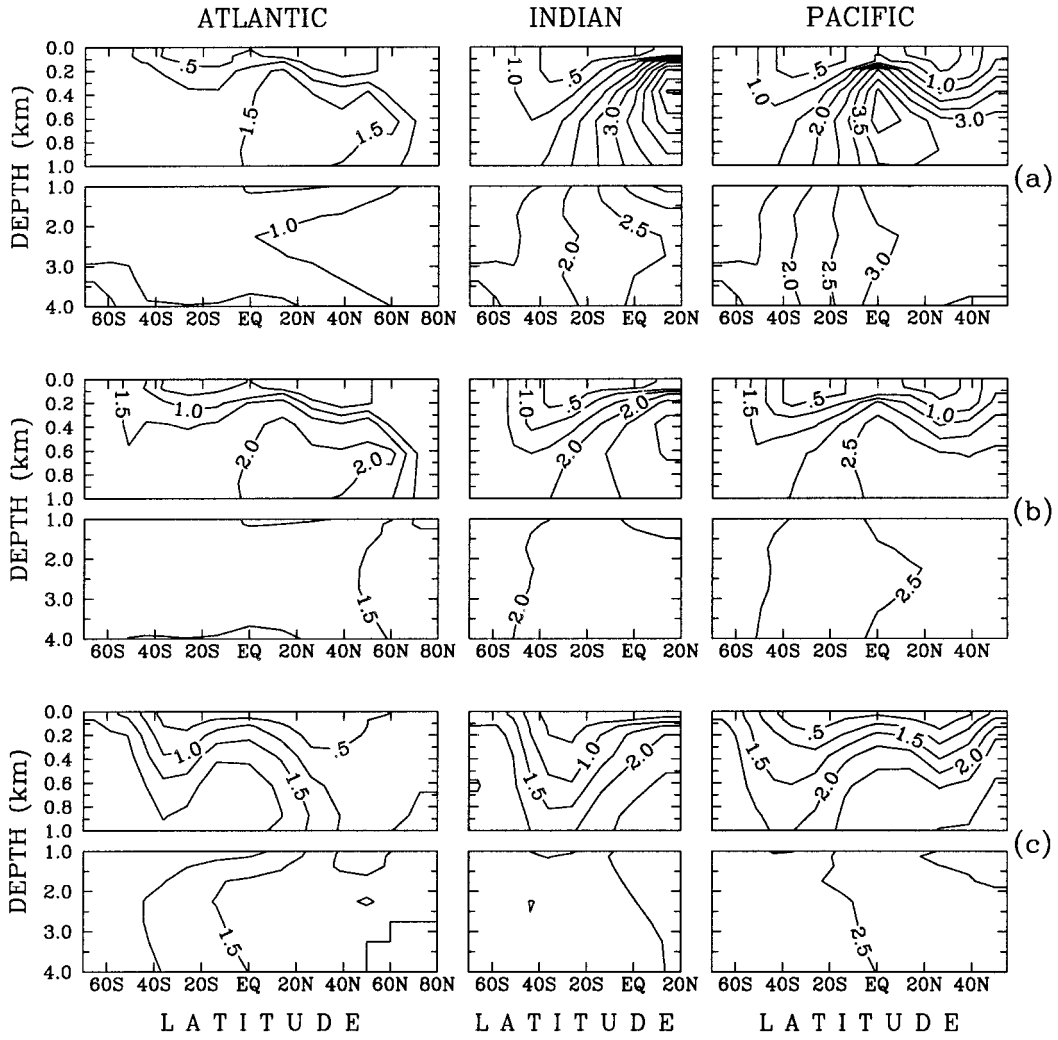

Fig. 3. Latitude-depth distribution of phosphate (mmol m^{-3}) in the three main oceanic basins. (a) POC-only model, (b) POC + DOC_l model, and (c) distributions established by zonally averaging and interpolating the climatological data of Conkright et al. (1994) onto the model grid. Contour interval is 0.5 mmol m^{-3}.

of 2 for $\sigma = 0.5$, because the feedback mechanism for producing nutrient trapping in those areas is substantially, if not completely reduced. Inspection of the circulation regime simulated in the equatorial Pacific and Indian (Wright and Stocker, 1992) indicates that DOC_l produced in those areas is exported by Ekman divergence. The highest inventories of DOC_l in the euphotic zone are not located in equatorial regions where maxima of DOC_l production are simulated (Fig. 6d). Instead, these inventories are found within the bordering subtropical areas where the model predicts minima in new production. The relatively low DOC_l inventories in the equatorial regions reflect the upwelling of low DOC_l waters to the surface (Najjar et al., 1992). The relatively high inventories in the subtropical areas, on the other hand, reflect the wind-driven input of DOC_l-rich waters from both the equator and the subpolar regions where secondary maxima in new production are pre-

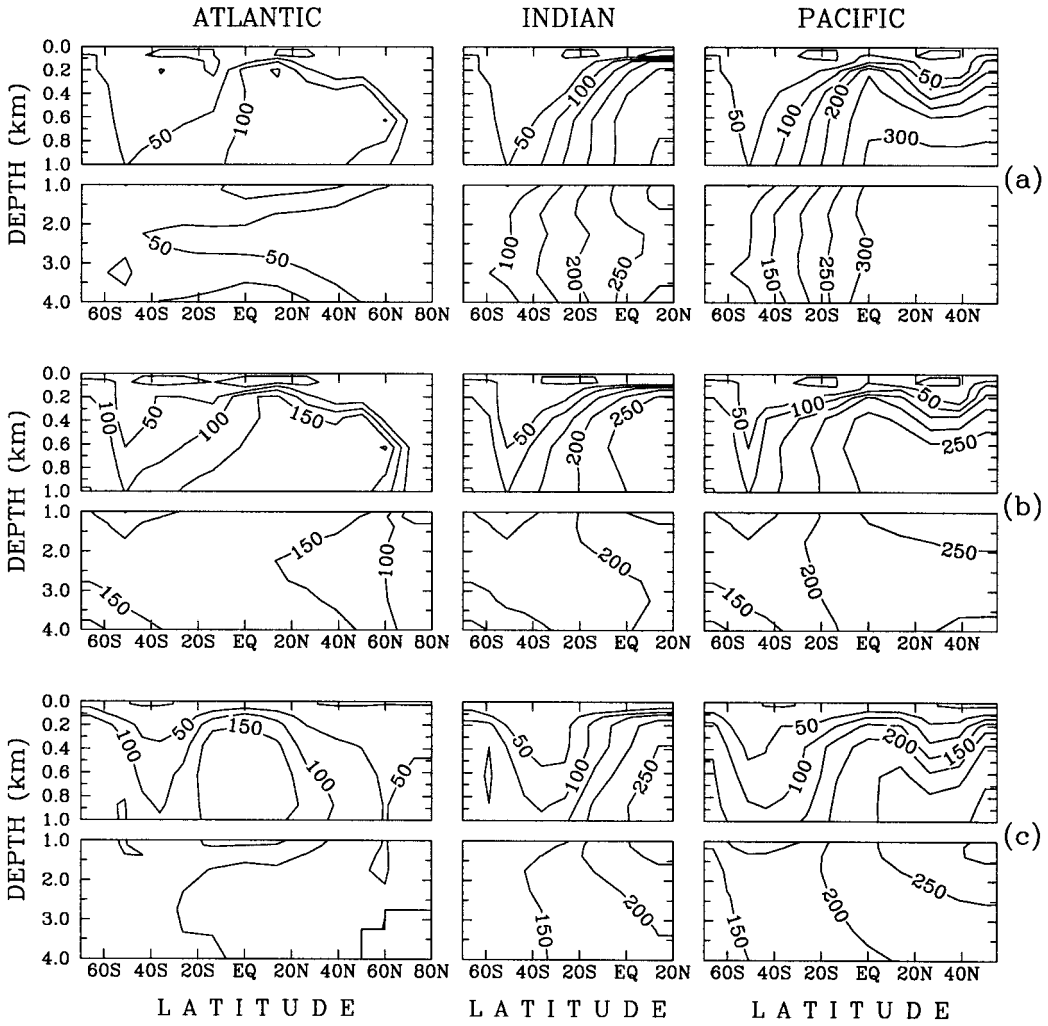

Fig. 4. Latitude-depth distribution of apparent oxygen utilization AOU (mmol m^{-3}) in the three main oceanic basins. (a) POC-only model, (b) POC + DOC_l model, and (c) distributions established by zonally averaging and interpolating the climatological data of Levitus and Boyer (1994b) onto the model grid. Contour interval is 50 mmol m^{-3}.

dicted. This input is balanced in the model by the downward export of DOC_l to the aphotic zone by Ekman pumping.

Another effect of including DOC_l in the model is an increase in new production at mid and subpolar latitudes (except in the North Pacific where this production is weakly affected; Fig. 6a–c). Everywhere south of 47.5°S, the POC-only model predicts the absence of new production because $PO_4 < PO_4^r$ in this area (Fig. 2). Clearly, the higher new production simulated at subpolar and polar latitudes by the POC + DOC_l model is due to the higher PO_4 content of the surface waters at these latitudes. From Fig. 3 we infer that this is ultimately related to the fact that much less phosphate is trapped within the tropical belts when a fraction of organic matter is allowed to be transported as DOC_l. This explains why rms(PO_4)

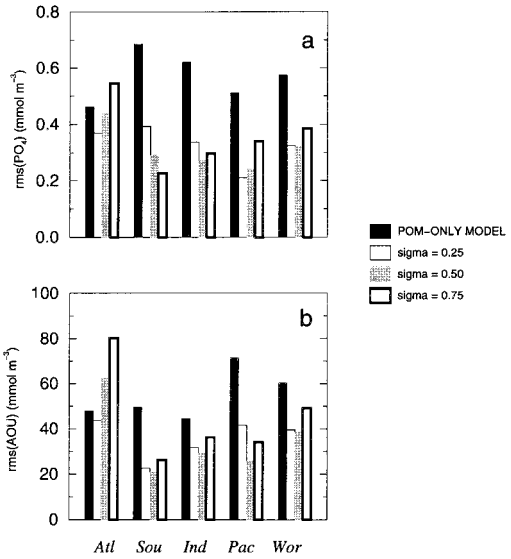

Fig. 5. Basin mean root-mean-square deviations produced on the distributions of (a) PO_4 and (b) AOU by the POC-only model and $POC + DOC_l$ model with different σ. Deviations are calculated relative to the observed PO_4 and AOU distributions reported in Figs. 3c and 4c, respectively.

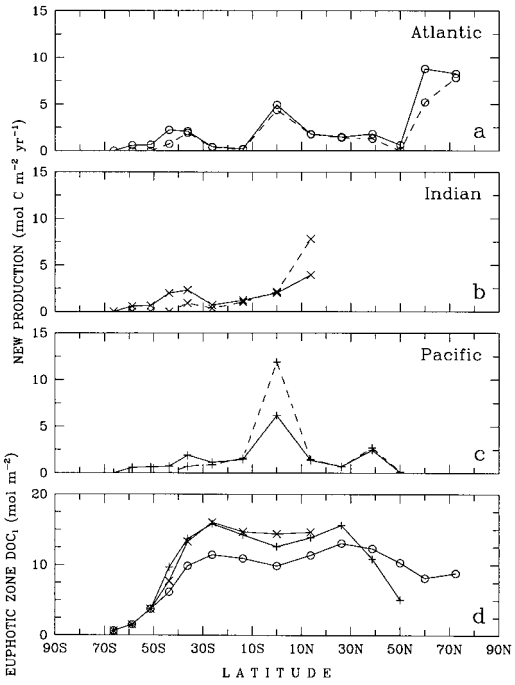

Fig. 6. (a–c) New production in the euphotic zone (top 100 m) in the three main oceanic basins predicted by the POC-only model (– – –) and $POC + DOC_l$ model (———). (d) Inventory of DOC_l in the euphotic zone of the Atlantic (○), Indian (×) and Pacific (+) simulated with $\sigma = 0.5$ and $\overline{DOC_l} = 10$ mmol m^{-3}.

and rms(AOU) in the Southern Ocean are strongly reduced (Fig. 5a,b). In the simulations that follow, σ is fixed to 0.5.

3.1.2. Total inventory of DOC_l. For two additional simulations with $\overline{DOC_l} = 5$ mmol m^{-3} and 20 mmol m^{-3}, rms(PO_4) and rms(AOU) are calculated as above. Compared to the POC-only model, rms(PO_4) is reduced for all the values of $\overline{DOC_l}$ considered. In each basin except the Atlantic, this reduction reaches a factor of 2 at least (Fig. 7a). More realistic values of AOU result in all cases except for the Atlantic with $\overline{DOC_l} = 10$ mmol m^{-3} and 20 mmol m^{-3} (Fig. 7b). In all the simulations that follow, $\overline{DOC_l}$ is fixed to 10 mmol m^{-3}.

3.2. Simulation of DIC, ALK and $\delta^{13}C_{DIC}$

The distributions of total dissolved inorganic carbon and alkalinity in the model are influenced by the cycling of organic matter and $CaCO_3$. The distribution of DIC is further affected by the air-sea exchange of CO_2. We examine the sensitivity of the distributions of DIC and ALK to the production ratio and the length scale for $CaCO_3$ dissolution. Unless stated otherwise, the coefficient for CO_2 transfer at the sea surface μ is fixed to a constant value of 67 mmol m^{-2} yr^{-1} μatm^{-1} (Broecker et al., 1985b). To reach steady state, the atmospheric boundary condition for DIC is $pCO_2^a = 280$ μatm (Barnola et al., 1987; Neftel et al., 1988). We compare model results with GEOSECS (1987) and TTO (1986) observations by considering the anthropogenic increase of pCO_2^a for the last 175 yr of integration according to data for the 1800–1975 period (Fig. B.1 in Enting et al., 1994). The ocean mean alkalinity, $\overline{ALK}$, is fixed to 2460 meq m^{-3} based on GEOSECS (1987) data (assuming a reference density of 1028 kg m^{-3} for seawater and an ocean mean salinity of 34.73).

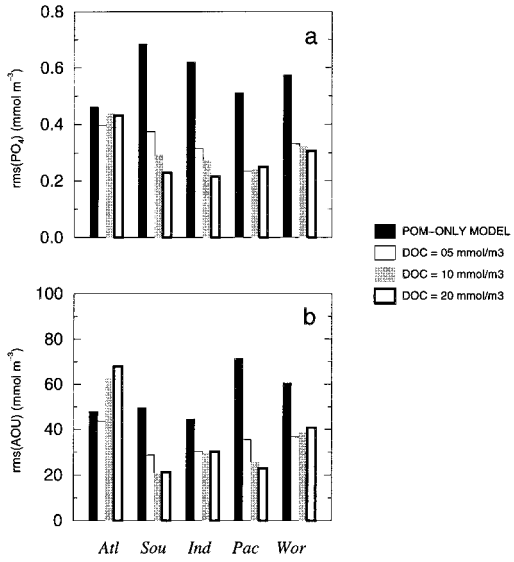

Fig. 7. Basin mean root-mean-square deviations produced on the distributions of (a) PO_4 and (b) AOU by the POC-only model and $POC + DOC_l$ model with different $\overline{DOC_l}$. Deviations are calculated relative to the observed PO_4 and AOU distributions reported in Figs. 3c and 4c, respectively.

3.2.1. Production ratio. Since the ocean mean production ratio $\overline{r_p}$ includes DOC_l formation, it should theoretically be lower than the ocean mean rain ratio. Based on nutrient data from GEOSECS stations, Broecker (1982) inferred that the best estimate of the ocean mean rain ratio is 0.25 ± 0.1. From other field data and a scaling analysis, Yamanaka and Tajika (1996) argued more recently, however, that this ratio should rather be between 0.08–0.10.

The ocean mean production ratio r_p in the model has a direct influence on DIC and ALK in the euphotic zone. Fig. 8 displays the meridional distributions of the DIC and ALK in the euphotic zone simulated with $\overline{r_p} = 0.03$, 0.06 and 0.12 (with the other biogeochemical parameters in Table 2). The simulation with $\overline{r_p} = 0.03$ (0.12) is characterized by DIC and ALK values which are too high (low) compared to GEOSECS + TTO averages. Using a value of 0.06 for $\overline{r_p}$ produces a remarkably consistent simulation of DIC and ALK, except at about 50°N in the Atlantic in the case of DIC. This value of $\overline{r_p}$ is lower, as it might be expected, than estimates of 0.08–0.25 reported in the literature for the ocean mean rain ratio. In the simulations that follow, $\overline{r_p}$ is fixed to 0.06.

3.2.2. Length scale for $CaCO_3$ dissolution. The effect of L_{dis} in the model is best demonstrated by considering the vertical distributions of DIC and ALK. We consider the basin mean vertical profiles of DIC and ALK with $L_{dis} = 2000$ m, 3000 m and 4000 m. The vertical profiles of DIC are fairly insensitive to L_{dis} and all are in close agreement with the data except for the Southern Ocean (Fig. 9a for $L_{dis} = 3000$ m). The low sensitivity of DIC profiles to L_{dis} stems from the fact DIC production at depth is mostly due to the oxidation of organic matter, rather than to the dissolution of $CaCO_3$. Because ALK is more sensitive than DIC to the cycle of $CaCO_3$, L_{dis} has a larger impact on the vertical distribution of alkalinity (Fig. 9b). With $L_{dis} = 4000$ m (deep $CaCO_3$ dissolution), ALK is generally too low in the Atlantic and the Southern Ocean and too high in the deep Pacific. Taking $L_{dis} = 2000$ m (shallow $CaCO_3$ dissolution) corrects these discrepancies to a large extent, but ALK excesses are now produced by the model at shallow depths in the Pacific and Indian. With an intermediate $L_{dis} = 3000$ m, ALK is again too low in the Atlantic and the Southern Ocean and too high in the deep Pacific. In the simulations of the cycle of $\delta^{13}C_{DIC}$ (see below), L_{dis} is fixed to this value.

3.2.3. Fractionation factor for photosynthesis. The cycle of $\delta^{13}C_{DIC}$ in our model is affected by the strong isotopic selectivity during photosynthesis and gas exchange. We assume no isotopic fractionation for calcification, $\alpha_{car} = 1$. This is a reasonable assumption given the small isotope effects (<3‰) for calcite and aragonite reported in the literature (Mook, 1986). This assumption is further supported by the tight correlation between $\delta^{13}C_{DIC}$ and PO_4 (primarily affected by organic matter cycling) in deep ocean waters (Kroopnick, 1985). The atmospheric boundary condition for calculating $DI^{13}C$, on the other hand, is fixed to $\delta^{13}C = -6.5$‰) (Friedli et al., 1986; Leuenberger et al., 1992). For a consistent comparison of model results with GEOSECS (1987) observations, however, $\delta^{13}C$ of atmospheric CO_2 is modified for the last 175 yr of integration according to a spline fit to data for the 1800–1975 period from the Siple

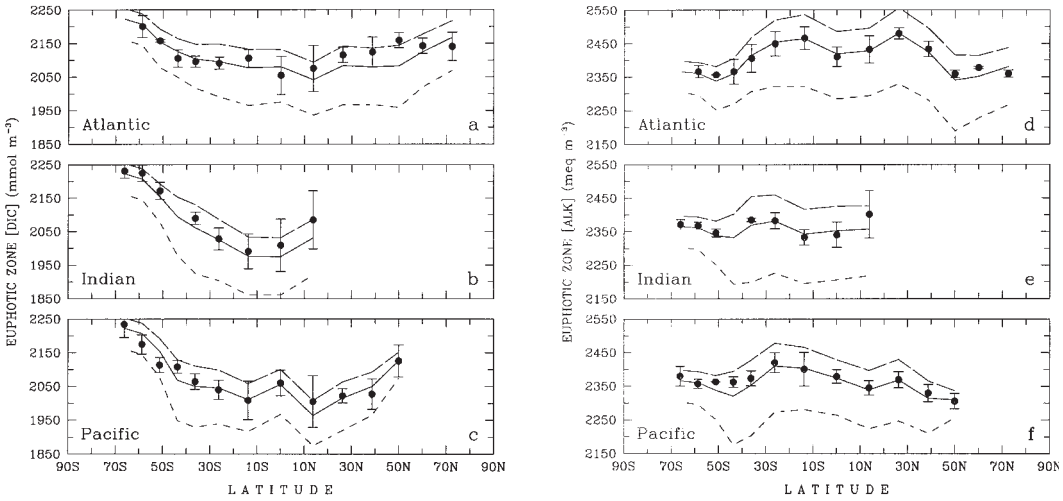

Fig. 8. Zonal mean concentration of (a–c) dissolved inorganic carbon and (d–f) alkalinity in the top 100 m in three main oceanic basins. Dots (●) are zonal averages computed from GEOSECS (1987) and TTO (1986) data (TTO stations 124, 143, 148 in the northern North Atlantic where DIC and ALK data from the GEOSECS expedition are not available). Vertical bars denote 1 standard deviation. The three curves are model results with $\overline{r_p} = 0.03$ (— — —), 0.06 (———) and 0.12 (– – –).

ice core (Friedli et al., 1986) and Cape Grim (Francey et al., 1995).

The fractionation factor between organic carbon and DIC for aquatic photosynthesis is defined as:

$$\alpha_{org} = \frac{\delta^{13}C_{org} + 1000‰}{\delta^{13}C_{DIC} + 1000‰}, \quad (39)$$

where $\delta^{13}C_{org}$ and $\delta^{13}C_{DIC}$ (both in ‰) are the isotopic ratios normalized to the standard PDB of organic C and DIC, respectively. According to data of $\delta^{13}C_{org}$ of suspended POM in ocean surface waters (Freeman and Hayes, 1992; Goericke and Fry, 1994), $\delta^{13}C_{org}$ varies mainly from −32‰ to −18‰. $\delta^{13}C_{DIC}$ measured on surface GEOSECS (1987) samples, on the other hand, fluctuates in a narrow range, i.e., between 0.5 to 2.5‰. From (39), the fractionation factor for marine photosynthesis should thus vary between 0.966 to 0.982. In a first simulation, we adopt a central value $\alpha_{org} = 0.975$.

Several studies have indicated a trend of decreasing $\delta^{13}C_{org}$ of suspended POM with decreasing concentration of aqueous CO_2 in ocean surface waters (Rau et al., 1989; Freeman and Hayes, 1992; Goericke and Fry, 1994). Based on a model of carbon photosynthetic fixation by microalgae, this trend has theoretical support (Rau et al., 1992). From data collected in the South Atlantic, the Southern Ocean and the Weddel Sea, Rau et al. (1989) established the following empirical relationship between $\delta^{13}C_{org}$ of suspended POM and CO_2(aq):

$$\delta^{13}C_{org} = -0.8‰\ \text{mmol}^{-1}\ \text{m}^3\ CO_2(\text{aq}) - 12.6‰, \quad (40)$$

where $\delta^{13}C_{org}$ is in ‰ and CO_2(aq) is in mmol m^{-3}. In a 2nd simulation, this relationship and the local $\delta^{13}C_{DIC}$ predicted by the model are included in eq. (39) to calculate a variable α_{org}.

Because $\alpha_{org} < 1$, light carbon is preferentially taken up during photosynthesis in surface waters and released during organic matter oxidation in deep waters. Therefore, α_{org} has a large influence on the vertical distribution of $\delta^{13}C_{DIC}$. Fig. 9c compares the basin mean vertical profiles of $\delta^{13}C_{DIC}$ simulated with a constant $\alpha_{org} = 0.975$ with GEOSECS (1987) data. The profiles are broadly consistent with the observations in each oceanic basin, i.e., the vertical gradients observed between surface and deep ocean $\delta^{13}C_{DIC}$ are generally captured. However, several discrepancies between the model and the data are found, including $\delta^{13}C_{DIC}$ underestimation in the upper kilo-

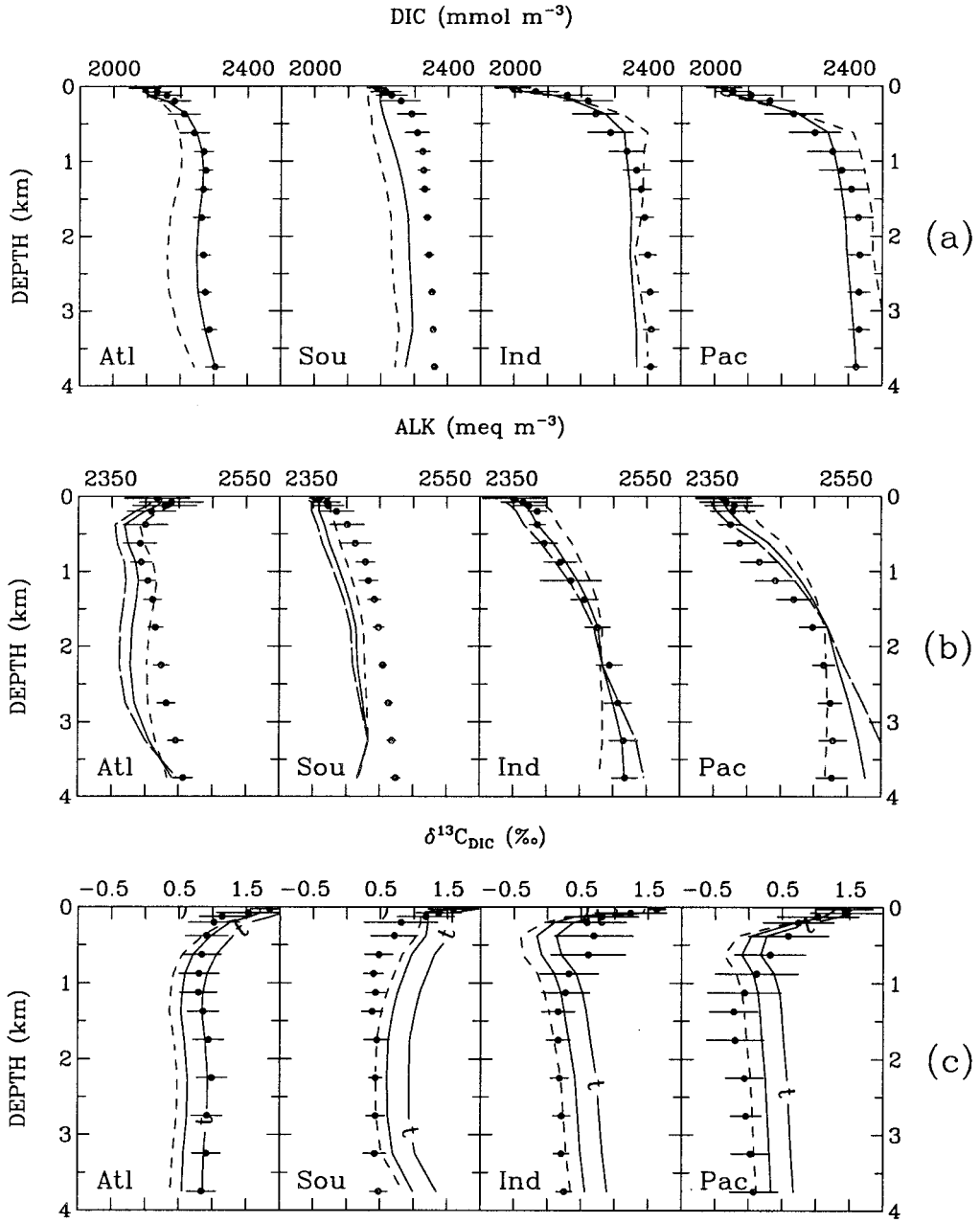

Fig. 9. Basin mean vertical profiles of (a) dissolved inorganic carbon, (b) alkalinity, and (c) δ^{13}C of DIC. Dots (●) are averages from GEOSECS (1987) and TTO (1986) data (same TTO stations as in Fig. 8; no $\delta^{13}C_{DIC}$ data from TTO). Horizonal bars denote 1 standard deviation. Results from (a) POC-only model (– – –) and POC + DOC$_l$ model (———), (b) POC + DOC$_l$ model with $L_{dis} = 2000$ (– – –), 3000 (———) and 4000 m (— — —) and (c) POC + DOC$_l$ model with a constant α_{org} (– – –), variable α_{org} (———), and a variable α_{org} and variable μ (— t —) are shown.

meter of the Indian and in the deep Atlantic. We analyse them below.

In the upper Indian, the model produces a pronounced $\delta^{13}C_{DIC}$ minimum which is shallower than in the data. A shallow $\delta^{13}C_{DIC}$ minimum is also simulated in the upper Pacific, but this is deeper than simulated in the upper Indian. Inspection of the distribution of the different water types in the model (not shown) indicates that waters north of 47.5°S in the Indian are a mixture of Central Waters (formed in the model between 47.5°S–32.5°N in each basin), Antarctic Intermediate Water (between 62.5°S–47.5°S in the Southern Ocean) and North Atlantic Deep Water (NADW, between 55°N–80°N in the Atlantic). At the locations where these waters are formed, the model $\delta^{13}C_{DIC}$ is generally too low compared to GEOSECS (1987) data (Fig. 10). Thus, a possible explanation for the $\delta^{13}C_{DIC}$ deficit in the upper Indian is too low preformed $\delta^{13}C_{DIC}$. Figs. 3b and 4b show that PO_4 and AOU excesses in the upper Indian are still present in the $POC + DOC_l$ model. On average, the PO_4 excess amounts to about 0.6 mmol m^{-3} associated with a theoretical

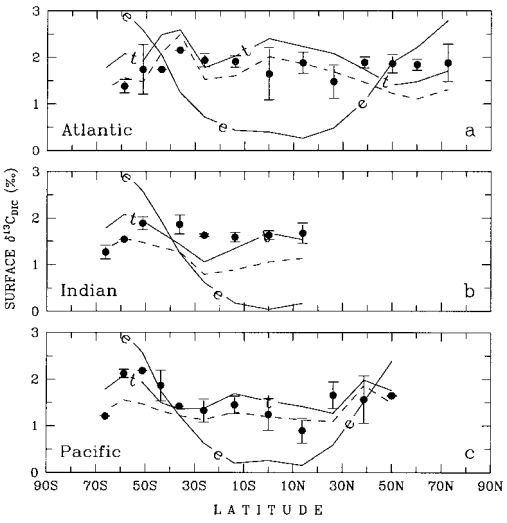

Fig. 10. Zonal mean $\delta^{13}C$ of surface DIC in the three main oceanic basins. Dots (●) are averages of GEOSECS (1987) data and horizonal bars denote 1 standard deviation. Values simulated with a constant $\alpha_{org} = 0.975$ (– – –), a variable α_{org} and variable μ (— t —) and $\delta^{13}C_{eq}$ expected from complete isotopic equilibrium with the atmosphere (— e —) are shown.

$\delta^{13}C_{DIC}$ underprediction of about 0.7‰ (Broecker and Maier-Reimer, 1992). Thus, excess remineralization of organic C (producing isotopically light DIC) could also explain the $\delta^{13}C_{DIC}$ deficit produced in the upper Indian.

The model further underestimates $\delta^{13}C_{DIC}$ in the deep Atlantic, although here the maximum difference between the basin averages of the model and the data (<0.5‰) is less than that produced in the upper Indian. Waters in the deep Atlantic are strongly dominated in the model by NADW (not shown). Thus, the $\delta^{13}C_{DIC}$ deficit there could also be explained by too low preformed $\delta^{13}C_{DIC}$ (Fig. 10a). However, PO_4 and AOU excesses are present also in the deep Atlantic in the $POC + DOC_l$ model (Figs. 3b, 4b). On average, the PO_4 excess reaches approximately 0.4 mmol m^{-3} which would translate into a theoretical underprediction of $\delta^{13}C_{DIC}$ of about 0.4‰. Thus, both errors in preformed $\delta^{13}C_{DIC}$ and a too high production of isotopically light DIC at depth are also likely candidates to explain the $\delta^{13}C_{DIC}$ deficit simulated in the deep Atlantic.

Because $\delta^{13}C_{DIC}$ is a central variable in paleoclimate studies, we give some further consideration to the $\delta^{13}C_{DIC}$ deficits produced by the model. Fig. 10 also gives the $\delta^{13}C_{DIC}$ expected from a complete isotopic equilibration with the atmosphere, $\delta^{13}C_{eq}$. Due to the increase of $\delta^{13}C_{eq}$ with decreasing temperature (Zhang et al., 1995), $\delta^{13}C_{eq}$ is small at low latitudes and large at high latitudes, with a peak-to-peak amplitude of about 3‰ in each oceanic basin. By contrast, $\delta^{13}C_{DIC}$ in the model exhibits a different meridional pattern and varies with peak-to-peak amplitudes of only about 1‰. This illustrates that the tendency towards isotopic equilibrium is largely offset, i.e. the preformed $\delta^{13}C_{DIC}$ in the model results from a subtle balance between compensatory effects associated with photosynthesis, gas exchange and/or the oceanic transport of carbon isotopes.

In a first attempt to improve the simulation, we use the variable fractionation factor for photosynthesis (eq. (40)). In this case, $\delta^{13}C_{DIC}$ come into better agreement with the data in the upper Indian and the deep Atlantic (Fig. 9c). As the cycling of organic matter and the circulation are exactly the same as with a constant α_{org}, the reason for this improvement must be related to preformed values of $\delta^{13}C_{DIC}$ in the different end-members. Due to an enhanced photosynthetic fractionation in cold

waters when using (40), the preformed $\delta^{13}C_{DIC}$ simulated with a variable α_{org} is indeed slightly greater (0.1–0.2‰) at the locations where NADW and AAIW are formed (not shown). However, the $\delta^{13}C_{DIC}$ simulated with a variable α_{org} is now too high in deep waters of the Southern Ocean, the Indian and the Pacific (Fig. 9c). Model-data discrepancies are, nevertheless, minor here (less than 0.2‰) and might not be significant given the variability of $\delta^{13}C_{DIC}$ in these waters.

In an attempt to reduce the deficits in surface $\delta^{13}C_{DIC}$ produced in the Indian and northern North Atlantic (0.5–0.8‰ in Fig. 10a,b), we use, in conjunction with a variable α_{org}, a variable μ computed from annual zonal averages of wind speed using the formula of Tans et al. (1990). A better fit to surface $\delta^{13}C_{DIC}$ data in these areas is produced in this case (Fig. 10a,b). A variable μ, however, also affects the vertical distribution of $\delta^{13}C_{DIC}$ in each oceanic basin (Fig. 9c). It still improves the simulation in the upper Indian and deep Atlantic but enhances $\delta^{13}C_{DIC}$ excesses produced in the Southern Ocean and in the deep Pacific and Indian with a variable α_{org} (Fig. 9c). All these changes result from the higher preformed $\delta^{13}C_{DIC}$ in the main water masses which ventilate deep levels in the model (e.g. NADW, Antarctic Bottom and Intermediate Waters). In summary, improvements in the prediction of $\delta^{13}C_{DIC}$ in one region of the world ocean by changing the value of a biogeochemical parameter often lead to degradation in another. This will be discussed in Section 4 in the context of potential shortcomings in the modelled circulation.

3.2.4. Air-sea difference of pCO_2. The air-sea difference in the partial pressure of CO_2 (ΔpCO_2) is a key aspect to validate ocean carbon cycle models (e.g. Sarmiento et al., 1995). Fig. 11 shows the meridional distributions of ΔpCO_2 simulated with a constant and variable μ (with the other biogeochemical parameters in Table 2). These distributions locate the sinks and sources for atmospheric CO_2 at the end of the transient simulation where the pCO_2^a record for the 1800–1975 period is prescribed. Annual zonal averages of ΔpCO_2 determined from field data are also given (from Broecker et al., 1986). Supersaturation is mostly simulated close to the equator whereas undersaturation is predicted primarily in the subtropical and subpolar regions. The more negative ΔpCO_2

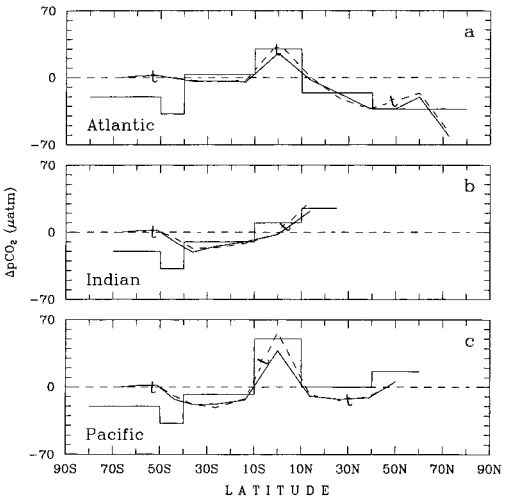

Fig. 11. Difference between the partial pressure of CO_2 in the surface water and in the atmosphere in the three main oceanic basins. Annual zonal averages estimated from field data are reported by the stair-like curves (from Fig. 1 of Broecker et al., 1986). Model results with a constant μ (– – –) and variable μ (— t —) are shown.

are found in the northern North Atlantic (Fig. 11). The distributions of ΔpCO_2 in the model are generally consistent with the observations, but large discrepancies occur south of 40°S and in the North Pacific. South of 40°S, the data indicate CO_2 undersaturation from -40 to -20 μatm, whereas the model generally predicts a slight supersaturation of less than 5 μatm (with both a constant and variable μ). In the North Pacific, on the other hand, the simulations with a constant and variable μ both consistently underestimate ΔpCO_2 by about 10 μatm on the average. The surface T, S, DIC and ALK simulated in these two regions are in relatively close agreement with the data (T and S are restored to climatological means, whereas DIC and ALK compare favourably with the observed zonal averages; solid line in Fig. 8). Thus, we would have anticipated that the ΔpCO_2 predicted by the model in these regions are also consistent with the observed estimates. However, there are numerous sources of discrepancy between the simulated and observed ΔpCO_2 in Fig. 11, including, e.g., shortcomings in the model which are not apparent from the compar-

ison with the (spatially and temporally limited) GEOSECS + TTO and even climatological data, and/or the geographic and seasonal biases in the ΔpCO_2 data.

4. Discussion

4.1. Model strengths

The distributions of PO_4 and AOU in the world oceans simulated by the "2.5-d" model are generally greatly improved when DOC_l is included, independent of σ or $\overline{DOC_l}$. In our model simulations, the lifetime of DOC_l $(1/\kappa)$ ranged from a minimum of 9 yr (with $\sigma = 0.5$ and $\overline{DOC_l} = 5$ mmol m^{-3}) to a maximum of 88 yr (with $\sigma = 0.5$ and $\overline{DOC_l} = 20$ mmol m^{-3}) (Table 3). These values are smaller but not inconsistent with the lifetimes of 50 yr and 314 yr for labile dissolved organic matter in previous model simulations including a constant κ (Bacastow and Maier-Reimer, 1991; Najjar et al., 1992). All these model values are higher than the turnover times of several days to several weeks observed in microbial utilization experiments (Amon and Benner, 1994) and derived from $^{234}Th:^{238}U$ disequilibria (Santschi et al., 1995). They are also higher than the seasonal turnover time of the DOC which is observed to accumulate in the upper water column during the stratification period in spring and to be mixed downward during the convection period in winter at temperate latitudes (Carlson et al., 1994). These model values are lower, on the other hand, than apparent ^{14}C ages > 1000 yr determined for DOC collected in the depth range 0–900 m in the central-north Pacific and Sargasso Sea (Williams and Druffel, 1987; Bauer et al., 1992). The large discrepancy between turnover rates in the model and those determined experimentally is related, at least partly, to the fact that DOC in ocean waters comprises several components characterized by very different labilities (as reflected, e.g., in the very distinct residence times inferred from laboratory microbial experiments and ^{14}C measurements on DOC collected in situ). A more realistic representation of DOC cycling in ocean biogeochemical models should thus include several classes of DOC with very different turnover rates (Kirchman et al., 1993; Yamanaka and Tajika, 1997).

Table 3. *Lifetime of DOC_l in the different model simulations*

$\overline{DOC_l}$ (mmol m^{-3})	σ (1)	$1/\kappa$ (yr)
10	0.25	70
10	0.50	30
10	0.75	15
5	0.5	9
10	0.5	30
20	0.5	88

In our model, the prediction of PO_4 and AOU in the Southern Ocean, the Indian and the Pacific is largely improved when DOC_l is included. This is associated with a reduction of nutrient trapping in the equatorial Indian and Pacific. This reduction is due to DOC_l export from these regions by Ekman divergence and subsequent pumping of DOC_l-rich water to depth in the bordering subtropical areas. In the Atlantic, by contrast, there is no strong nutrient trapping in the POC-only model, and rms(PO_4) and rms(AOU) drop only slightly or are even larger when DOC_l is included. The absence of a strong nutrient trapping in the equatorial Atlantic seems related to the fact that the thermohaline flow simulated in the upper kilometer in this basin is mostly horizontal (Wright and Stocker, 1992). This flow would not permit the formation of local nutrient excesses according to the feedback mechanism discussed by Najjar et al. (1992) which rather requires a dominant upwelling. This would hence explain why in the POC-only model the new production in the equatorial Atlantic is lower than that in the equatorial Indian and Pacific (Fig. 6).

In addition to PO_4 and AOU, the major features in the distributions of DIC, ALK and $\delta^{13}C_{DIC}$ in the modern oceans are captured by our model when DOC_l is included. For instance, inclusion of DOC_l corrects to a large extent major discrepancies produced by the POC-only model relative to the DIC data (Fig. 9a). These include DIC deficits in the Atlantic and Southern Ocean and DIC excesses in the deep Pacific. In the Indian, on the other hand, the POC-only model produces slightly better results.

With the set of standard parameters in Tables 1 and 2, the predicted total inventory of DIC is

about 38 705 GtC in the preindustrial ocean and 38 791 GtC for the year 1985. The first value is in excellent agreement with the observed estimate of 39 000 GtC for the preindustrial ocean. The difference of 86 GtC, on the other hand, is about 30% lower than the estimate of 120 GtC for the accumulation of anthropogenic CO_2 from the preindustrial era to the decade 1980–1989 (Siegenthaler and Sarmiento, 1993). The cumulative uptake of CO_2 for the period from 1770 to 1980 is 78 GtC (calculated by prescribing for that period the same pCO_2^a record as above) and the invasion flux of CO_2 into the ocean for the year 1980 is 1.36 GtC yr^{-1}. These values are lower than estimates of 92–123 GtC and 1.67–2.25 GtC yr^{-1} from models of varying complexity (Table 4 in Stocker et al., 1994). This is most likely due to the relatively small vertical diffusivity adopted in our simulations ($K_v = 2 \cdot 10^{-5}$ m^2 s^{-1} versus $4 \cdot 10^{-5}$ m^2 s^{-1} in Stocker et al. (1994) which gave values of 1.91 GtC yr^{-1} and 100 GtC). Finally, the rate of new production predicted for the world ocean is 8.8–9.6 GtC yr^{-1} in the POC-only model (with the range depending on τ_{PO_4}). It is 6.3–10.8 GtC yr^{-1} in the $POC + DOC_l$ model (depending on $\overline{DOC_l}$). All these rates are consistent with data- and model-based estimates between 3.4 to over 15 GtC yr^{-1} reported by Ducklow (1995).

4.2. *Model weaknesses*

4.2.1. Shortcomings in the modelled circulation. It is legitimate to consider whether the failures of the POC-only model to reproduce the observed PO_4 and AOU distributions result, at least partly, from shortcomings in the model circulation and resolution. Anderson and Sarmiento (1995), for instance, found that discrepancies in the PO_4 fields simulated by their 3-d model are mainly due to shortcomings of the modelled circulation, rather than the description of biological processes. Matear and Holloway (1995) further showed that the PO_4 field simulated in the North Pacific by their 3-d model is very sensitive to the modelled circulation and that a field consistent with the data can be reproduced with only small adjustments in this circulation. Finally, Najjar and Toggweiler (1993) mentioned that the 3-d models of Bacastow and Maier-Reimer (1991) and Najjar et al. (1992), which are characterized by nutrient trapping in their POM-only version, have a too coarse horizontal resolution (4°–5°) to properly resolve the important features of tropical ocean circulation.

Deficiencies in the modelled circulation are likely to contribute to discrepancies in the PO_4 fields simulated by our model (with a resolution of 12.5°–15° between 20°S–20°N). In this model, major discrepancies are related to nutrient trapping in the equatorial Indian and Pacific (Fig. 3a). There, the circulation is dominated by upwelling associated with two components: wind-driven divergence and thermohaline transport (Wright and Stocker, 1992). The thermohaline upwelling in the Indian and Pacific originates from the deepest levels of the water column. This is not consistent with tracer data which suggest that this upwelling is deflected as a southward flow at mid-depth in these basins (Broecker et al., 1985c; Toggweiler and Samuels, 1993). According to these data, the meridional circulation in the Indian and Pacific would be characterized by a two-cell structure rather than by a single top-to-bottom overturning. Interestingly, including in our model a depth-dependent vertical diffusivity according to the equation of Bryan and Lewis (1979) produces a southward flow at mid-depth in the Pacific (Stocker and Wright, 1996). Using $K_v(2500\ m) = 0.6 \cdot 10^{-4}$ m^2 s^{-1} in this equation with the other circulation parameters adopted here (Table 1) produces the same feature in the Pacific and basin mean vertical profiles of T, S and $\Delta^{14}C$ that are consistent with the data (not shown). However, the simulation with the depth-dependent K_v of Bryan and Lewis (1979) is characterized, when DOC_l is excluded, by a nutrient trapping in the Pacific and Indian which is even larger than in Fig. 3a. Thus, although the simulation with a southward flow at mid-depth in the Pacific may be more consistent with tracer data, it does not improve the prediction of biogeochemical tracers in this basin.

Two other results point to possible shortcomings in the modelled circulation. First, with the set of parameters in Tables 1 and 2, ALK excesses relative to the data are produced by the model in the deep Pacific (Fig. 9b). These excesses can be reduced by decreasing either the ocean mean production ratio $\overline{r_p}$ or the length scale for $CaCO_3$ dissolution L_{dis}. However, in the former case, the simulated DIC and ALK become too high in

the surface waters (Fig. 8 for $\overline{r_p} = 0.03$) and in the latter case, the simulated ALK become too high in the upper Pacific and Indian (Fig. 9b for $L_{dis} = 2000$ m). Second, using a variable coefficient for CO_2 transfer at the surface (μ) improves the simulation of $\delta^{13}C_{DIC}$ in the Atlantic and in the upper Indian and Pacific. However, this leads to $\delta^{13}C_{DIC}$ values in the deep Southern Ocean, Indian and Pacific that are less satisfactory than with a constant μ. These two examples illustrate that deficiencies in the modelled circulation might preclude a consistent simulation of ALK and $\delta^{13}C_{DIC}$.

4.2.2. Simplified treatment of the carbonate cycle. Our model assumes that all the organic matter and $CaCO_3$ particles are recycled in the water column. Although the first assumption is reasonable from oceanic budgets of organic C (Smith and Hollibaugh, 1993), the second is inconsistent with oceanic budgets of $CaCO_3$ which indicate that a significant fraction of the $CaCO_3$ precipitated in the deep sea is preserved in sediments (Milliman, 1993). Therefore, the assumption that no $CaCO_3$ is buried in deep sea sediments puts limitations to our model. A first limitation is that this model cannot address changes in the depth of the sedimentary lysocline documented for the late Pleistocene (Farrell and Prell, 1989). These changes occurred on a time scale of few thousand years (Broecker and Peng, 1987) and should have affected the concentration of atmospheric CO_2 (Broecker and Peng, 1987; Archer and Maier-Reimer, 1994). Another limitation concerns the redissolution of all the $CaCO_3$ reaching the ocean floor in the deepest grid cells. This creates an artificial source of alkalinity for the bottom waters in our model. For instance, with $L_{dis} =$ 3000 m, 28% of the $CaCO_3$ flux leaving the euphotic zone is redissolved in the deepest grid cells which is another explanation for ALK excesses in the deep Pacific (Fig. 9b). Thus, a more realistic description of the ocean carbonate cycle should account for the effects of $CaCO_3$ preservation in sediments.

4.3. A modification for paleoclimate studies

The ultimate goal with the model presented here is to investigate changes in the ocean carbon cycle and atmospheric pCO_2 due to changing ocean circulation. We therefore require a prognostic description in which new production depends on the surface concentration of a biolimiting nutrient (Siegenthaler and Wenk, 1984). Whether phosphate or nitrate plays this role is not important for our purpose provided that both nutrients are equally affected by circulation changes and related stoichiometrically in the deep sea (Tyrrell and Law, 1997).

The half-saturation constants for PO_4 uptake (K_{PO_4}) by natural phytoplankton assemblages reported by Nalewajko and Lean (1980) have a range of approximately one order of magnitude with a central value of about 0.4 mmol m^{-3}. The observed annual zonal averages of PO_4 in the euphotic zone, on the other hand, range from $\sim$0.1 to 2 mmol m^{-3} (Fig. 2). Thus, if saturation kinetics with a K_{PO_4} representative of natural phytoplankton reasonably describe the dependence of new production on ambient PO_4, the response of new production to a PO_4 change should be quite different in nutrient-depleted waters (e.g., in subtropical gyres) and nutrient-rich waters (e.g., at polar latitudes). In order to account for this, new production in the prognostic description ($J^{\mathscr{T}}_{org,p}$) is related to PO_4 using the Michaelis–Menten equation for uptake kinetics. The rate of $CaCO_3$ formation ($J^{\mathscr{T}}_{car,p}$) is inferred from the rate of new production via r_p as in eq. (3). Thus,

$$J^{\mathscr{T}}_{org,p} = r^{\mathscr{T}}_{org} J^{PO_4}_{org,pot} \frac{PO_4}{K_{PO_4} + PO_4}, \tag{41}$$

$$J^{\mathscr{T}}_{car,p} = r^{\mathscr{T}}_{car} r_p J^{DIC}_{org}, \tag{42}$$

where $r^{\mathscr{T}}_{org}$ and $r^{\mathscr{T}}_{car}$ are the same atomic ratios as above, and $J^{PO_4}_{org,pot}$ is a "potential" new production (expressed in P units). $J^{PO_4}_{org,pot}$ is defined as the production that would be achieved in a given oceanographic regime with unlimited supply of nutrients. Ideally, $J^{PO_4}_{org,pot}$ for the modern oceans should be such that the simulated meridional distributions of PO_4 in the euphotic layer remain close to the observations as in the diagnostic description of the biological activity (Fig. 2). From (41), this condition is satisfied if we choose:

$$J^{PO_4}_{org,pot} = J^{PO_4}_{org} \frac{K_{PO_4} + PO_4}{PO_4}, \tag{43}$$

i.e., the potential new production in the prognostic description could be derived from the steady state $J^{PO_4}_{org}$ diagnosed from restoring PO_4 to observed

PO_4^r. If $J^{PO_4}_{org,pot}$ values adopted in paleoclimatic simulations are constrained in this way, it is therefore assumed that the "potential new productions" were the same in the past as today.

5. Conclusions

We have embedded a simple description of the cycles of organic carbon and $CaCO_3$ into the zonally averaged, global ocean circulation model of Wright and Stocker (1992). This is the natural extension of previous studies that have used this model in order to get insight into the cycle of inorganic tracers in the oceans (Lehman et al., 1993; Stocker et al., 1994; Lynch-Stieglitz et al., 1995; Stocker and Wright, 1996). Here, the processes of photosynthesis and respiration and $CaCO_3$ production and dissolution are included. This has been based largely on previous efforts to simulate these processes in the world oceans (Najjar et al., 1992; Maier-Reimer, 1993; Yamanaka and Tajika, 1996). Yet, our model is unique in its "two-and-half" dimensional representation of the marine domain and constitutes a dynamical circulation-biogeochemical model intermediate between highly parameterized box models and expensive 3-d models. From systematic sensitivity experiments, an optimal set of values has been selected for the weakly constrained biogeochemical parameters (Table 2). Despite its inevitable simplicity, the "2.5-d" model is able to capture the large-scale distribution of PO_4, AOU, DIC, ALK and $\delta^{13}C_{DIC}$ in the modern oceans. As in 3-d models, inclusion of dissolved organic matter reduces nutrient trapping simulated below the highly productive equatorial regions. In our zonally averaged model, this is due to the export of DOC_l from these regions by wind-driven divergence and to the subsequent DOC_l pumping at depth in subtropical areas. Admittedly, the calibration of our model is primarily hinged on modern observations and no guarantee can be given whether it is also appropriate during entirely different climate periods. One has to cope with this difficulty, however, with any other model. Major discrepancies with tracer data have been identified and tentatively explained in order to highlight the possible improvements that could be introduced, if needed. In its present form, however, the model can serve as a highly efficient tool to test hypotheses regarding the variability of paleoclimate proxies recorded in deep sea sediments and polar ices (Marchal et al., 1998).

6. Acknowledgements

We are greatly indebted to two anonymous reviewers for careful and extensive comments on the paper which has improved the presentation. Thanks are due to M. Heimann who provided a composite record of $\Delta^{14}C$ of the industrial atmosphere and to N. Gruber for discussions. This study was made possible by the Swiss National Science Foundation and grant BBW 95.0471 from European Projects ENV4-CT95-0131 "Variability of the Glacial and Interglacial Climates and Abrupt Climatic Changes" and ENV4-CT95–0130 "North-South Climatic Connection and Carbon Cycle over the last 250 kyr".

REFERENCES

Amon, R. M. W. and Benner, R. 1994. Rapid recycling of high-molecular-weight dissolved organic matter in the ocean. *Nature* **369**, 549–552.

Anderson, L. A. and Sarmiento, J. L. 1994. Redfield ratios of remineralization determined by nutrient data analysis. *Global. Biogeochem. Cycles* **8**, 65–80.

Anderson, L. A. and Sarmiento, J. L. 1995. Global ocean phosphate and oxygen simulations. *Global. Biogeochem. Cycles* **9**, 621–636.

Archer, D. and Maier-Reimer, E. 1994. Effect of deep-sea sedimentary calcite preservation on atmospheric CO_2 concentration. *Nature* **367**, 260–263.

Bacastow, B. and Maier-Reimer, E. 1991. Dissolved organic carbon in modeling oceanic new production. *Global Biogeochem. Cycles* **5**, 71–85.

Barnola, J.-M., Raynaud, D., Korotkevich Y. S. and Lorius, C. 1987. Vostok ice core provides 160,000-year record of atmospheric CO_2. *Nature* **329**, 408–414.

Bauer, J. E., Williams P. M. and Druffel, E. R. M. 1992. ^{14}C activity of dissolved organic carbon fractions in the north-central Pacific and Sargasso Sea. *Nature* **357**, 667–670.

Bishop, J. K. B. 1989. Regional extremes in particulate matter composition and flux: effects on the chemistry of the ocean interior. In: *Productivity of the Ocean: present and past*, edited by Berger, W. H. Smetacek

V. S. and Wefer. G. New York. pp. 117–137. John Wiley.

Boyle, E. A. 1988. The role of vertical chemical fractionation in controlling late Quarternary atmospheric carbon dioxide. *J. Geophys. Res.* **93**, 15701–15714.

Boyle, E. A. and Keigwin, L. D. 1987. North atlantic thermohaline circulation during the past 20,000 years linked to high-latitude surface temperature. *Nature* **330**, 35–40.

Brewer, P. G. and Glover, D. M. 1987. Ocean chemical fluxes 1983–1986. *Rev. Geophys.* **25**, 1376–1386.

Broecker, W. S. 1982. Glacial to interglacial changes in ocean chemistry. *Prog. Oceanogr.* **11**, 151–197.

Broecker, W. A., and Denton, G. H. 1989. The role of ocean-atmosphere reorganizations in glacial cycles. *Geochim. Cosmochim. Acta* **53**, 2465–2501.

Broecker, W. S., Ledwell, J. R., Takahashi, T., Weiss, R., Merlivat, L., Memery, L., Peng, T.-H., Jähne, B. and Münnich, K. O. 1986. Isotopic versus micrometeorologic ocean CO_2 fluxes: a serious conflict. *J. Geophys. Res.* **91**, 10 517–10 527.

Broecker, W. A. and Maier-Reimer, E. 1992. The influence of air and sea exchange on the carbon isotope distribution in the sea. *Global Biogeochem. Cycles* **6**, 315–320.

Broecker, W. S. and Peng, T.-H. 1974. Gas exchange rates between air and sea. *Tellus* **26B**, 21–35.

Broecker, W. S. and Peng. T.-H. 1982. *Tracers in the sea.* Eldigio Press. Lamont-Doherty Geological Observatory, Palisades, NY.

Broecker, W. S. and Peng, T.-H. 1986. Glacial to interglacial changes in the operation of the global carbon cycle. *Radiocarbon* **28**, 309–327.

Broecker, W. S. and Peng, T.-H. 1987. The role of $CaCO_3$ compensation in the glacial to interglacial atmospheric CO_2 change. *Global Biogeochem. Cycles* **1**, 15–29.

Broecker, W. S., Peteet, D. and Rind, D. 1985a. Does the ocean-atmosphere system have more than one stable mode of operation? *Nature* **315**, 21–25.

Broecker, W. S., Peng, T.-H., Östlund, G. and Stuiver, M. 1985b. The distribution of bomb radiocarbon in the ocean. *J. Geophys. Res.* **90**, 6953–6970.

Broecker, W. S., Takahashi, T. and Takahashi, T. 1985c. Source and flow patterns of deep-ocean waters as deduced from potential temperature, salinity, and initial phosphate concentration. *J. Geophys. Res.* **90**, 6925–6939.

Bryan, K. and Lewis, L. J. 1979. A water mass model of the world ocean. *J. Geophys. Res.* **84**, 2503–2517.

Campbell, J. W. and Aarup, T. 1992. New production in the North Atlantic derived from seasonal patterns of surface chlorophyll. *Deep-Sea Res.* **39**, 1669–1694.

Carlson, C. A., Ducklow, H. W. and Michaels, A. F. 1994. Annual flux of dissolved organic carbon from the euphotic zone in the northwestern Sargasso Sea. *Nature* **371**, 405–408.

Codispoti, L. A. 1989. Phosphorus vs. nitrogen limitation of new and export production. In: *Productivity of the Ocean*: *present and past*, edited by Berger, W. H. Smetacek, V. S. and Wefer G. pp. 377–394. John Wiley & Sons. New York.

Conkright, M. E., Levitus, S. and Boyer, T. P. 1994. *World ocean atlas 1994, vol. 1: Nutrients.* Washington, D.C.: U.S. Department of Commerce, NOAA, NESDIS.

Copin-Montégut, G. and Avril, B. 1993. Vertical distribution and temporal variation of dissolved organic carbon in the North-Western Mediterranean Sea. *Deep-Sea Res.* **40**, 1963–1972.

Cortijo, E., Yiou, P., Labeyrie, L. and Cremer, M. 1995. Sedimentary record of rapid climatic variability in the North Atlantic during the last glacial cycle. *Paleoceanography* **10**, 911–926.

Craig, H. 1957. Isotopic standards for carbon and oxygen and correction factors for mass-spectrometric analysis of carbon dioxide. *Geochim. Cosmochim. Acta* **12**, 133–149.

Drange, H. 1994. *An isopycnic coordinate carbon cycle model for the North Atlantic*; *and the possibility of disposing of fossil fuel* CO_2 *in the ocean.* PhD thesis. Department of Mathematics, University of Bergen, Norway.

Ducklow, H. W. 1995. Ocean biogeochemical fluxes: New production and export of organic matter from the upper ocean. *Rev. Geophys.* (*suppl.*) 1271–1276.

Ducklow, H. W., Carlson, C. A., Bates, N. R., Knap, A. H. and Michaels, A. F. 1995. Dissolved organic carbon as a component of the biological pump in the North Atlantic ocean. *Philos. Trans. R. Soc.* (*Lond.*) **B 348**, 161–167.

Dugdale, R. and Goering, J. J. 1967. Uptake of new and regenerated forms of nitrogen in primary productivity. *Limnol. Oceanogr.* **12**, 196–206.

Enting, I. G., Wigley, T. M. L. and Heimann. M. 1994. *Future emissions and concentrations of carbon dioxide*: *Key ocean/atmosphere/land analyses.* CSIRO Division of Atmospheric Research Technical Paper No. 31. National Library of Australia Cataloguing-in-Publication Entry.

Falkowski, P. G. 1997. Evolution of the nitrogen cycle and its influence on the biological sequestration of CO_2 in the ocean. *Nature* **387**, 272–275.

Farrell, J. W. and Prell, W. L. 1989. Climatic change and $CaCO_3$ preservation: an 800,000 year bathymetric reconstruction from the central equatorial Pacific Ocean. *Paleoceanography* **4**, 447–466.

Francey, R. J., Tans, P. P., Allison, C. E., Enting, I. G., White, J. W. C. and Trolier, M. 1995. Changes in oceanic and terrestrial carbon uptake since 1982. *Nature* **373**, 326–330.

Freeman, K. H. and Hayes, J. M. 1992. Fractionation of carbon isotopes by phytoplankton and estimates of ancient CO_2 levels. *Global Biogeochem. Cycles* **6**, 185–198.

Friedli, H., Lotscher, H., Oeschger, H., Siegenthaler, U. and Stauffer, B. 1986. Ice core record of the $^{13}C/^{12}C$ ratio of atmospheric CO_2 in the past two centuries. *Nature* **324**, 237–238.

Gargett, A. E. and Holloway, G. 1984. Dissipation and diffusion by internal wave breaking. *J. Mar. Res.* **42**, 15–27.

GEOSECS, 1987. GEOSECS. *Atlantic, Pacific, and Indian ocean expeditions, vol. 7: Shoredbased data and graphics*. International Decade of Ocean Exploration. National Science Foundation.

Goericke, R. and Fry, B. 1994. Variations of marine plankton $\delta^{13}C$ with latitude, temperature, and dissolved CO_2 in the world ocean. *Global Biogeochem. Cycles* **8**, 85–90.

Gordon, A. L. 1986. Interocean exchange of thermocline water. *J. Geophys. Res.* **91**, 5037–5046.

Gregg, M. G. 1987. Diapycnal mixing in the thermocline: A review. *J. Geophys. Res.* **92**, 5249–5286.

Gruber, N. and Sarmiento, J. L. 1997. Global patterns of marine nitrogen fixation and denitrification. *Global Biogeochem. Cycles* **11**, 235–266.

Guo, L., Santschi, P. H. and Warnken, K. W. 1995. Dynamics of dissolved organic carbon (DOC) in oceanic environments. *Limnol. Oceanogr.* **40**, 1392–1403.

Han, Y. J. and Lee, S. W. 1983. An analysis of monthly mean windstress over the global ocean. *Mon. Weather Rev.* **111**, 1554–1566.

Hecky, R. E. and Kilham, P. 1988. Nutrient limitation of phytoplankton in freshwater and marine environments: A review of recent evidence on the effects of enrichment. *Limnol. Oceanogr.* **33**, 796–822.

Heinze, C. 1990. *Zur Erniedrigung des Atmosphärischen Kohlendioxigehalts durch den Weltozean während der letzten Eiszeit*. Max-Planck-Inst. für Meteorol., Hamburg, Germany. Tech. Rep. 3. pp. 1–180.

Honjo, S. 1990. Particle fluxes and modern sedimentation in the polar oceans. In: *Polar oceanography*, Part B: *Chemistry, biology and geology*, pp. 687–739. Academic Press.

Keigwin, L. D., Jones, G. A. and Lehman, S. J. 1991. Deglacial meltwater discharge, North Atlantic deep circulation and abrupt climate change. *J. Geophys. Res.* **96**, 16 811–16 826.

Keir, R. S. 1988. On the Late Pleistocene ocean geochemistry and circulation. *Paleoceanography* **3**, 413–445.

Keir, R. S. 1990. Reconstructing the ocean carbon system variation during the last 150,000 years according to the Antarctic nutrient hypothesis. *Paleoceanography* **5**, 253–276.

Kirchman, D. L., Lancelot, C., Fasham, M. J. R., Legendre, L., Radach, G. and Scott, M. 1993. Dissolved organic matter in biogeochemical models of the ocean. In: *Towards a model of ocean biogeochemical processes*, edited by Evans G. T. and Fasham M. J. R. Volume I 10 of NATO ASI. pp. 209–225. Springer-Verlag.

Kroopnick, P. M. 1985. The distribution of ^{13}C of TCO_2 in the world oceans. *Deep-Sea Research* **32**, 57–84.

Ledwell, J. R., Watson, A. J. and Law, C. S. 1993. Evidence for slow mixing across the pycnocline from an open-ocean tracer-release experiment. *Nature* **364**, 701–703.

Lehman, S. J., Wright, D. G. and Stocker, T. F. 1993. Transport of freshwater into the deep ocean by the conveyor. In: *Ice in the climate system*, edited by W. R. Peltier. NATO ASI Ser. I, 12. pp. 187–209.

Leuenberger, M., Siegenthaler, U. and Langway, C. C. 1992. Carbon isotope composition of atmospheric CO_2 from an antarctic ice core. *Nature* **357**, 488–490.

Levitus, S. and Boyer, T. P. 1994a. *World ocean atlas 1994, vol. 4: Temperature*. Washington, D.C.: U.S. Department of Commerce, NOAA, NESDIS.

Levitus, S. and Boyer, T. P. 1994b. *World ocean atlas 1994, vol. 2: Oxygen*. Washington, D.C.: U.S. Department of Commerce, NOAA, NESDIS.

Levitus, S., Burgett, R. and Boyer, T. P. 1994. *World ocean atlas 1994, vol. 4: Salinity*. Washington, D.C.: U.S. Department of Commerce, NOAA, NESDIS.

Lynch-Stieglitz, J., Stocker, T. F., Broecker, W. S. and Fairbanks, R. G. 1995. The influence of air-sea interaction on the isotopic composition of organic carbon: observations and modeling. *Global Biogeochem. Cycles* **9**, 653–665.

Machta, L. and Hughes, E. 1970. Atmospheric oxygen in 1976 and 1970. *Science* **168**, 1582–1584.

Maier-Reimer, E. 1993. Geochemical cycles in an ocean general circulation model. Preindustrial tracer distributions. *Global Biogeochem. Cycles* **7**, 645–677.

Marchal, O., Stocker, T. F. and Joos, F. 1998. Impact of oceanic reorganizations on the ocean carbon cycle and atmospheric carbon dioxide content. *Paleoceanography*, in press.

Martin, J. H. and Fitzwater, S. E. 1992. Dissolved organic carbon in the Atlantic, Southern and Pacific oceans. *Nature* **356**, 699–700.

Martin, J. H., Knauer, G. A., Karl, D. M. and Broenkow, W. W. 1987. VERTEX: carbon cycling in the northeast Pacific. *Deep-Sea Res.* **34**, 267–285.

Martin, J. H., Fitzwater, S. E., Michael Gordon, R., Hunter, C. N. and Tanner, S. J. 1993. Iron, primary production and carbon-nitrogen flux studies during the JGOFS North Atlantic Bloom Experiment. *Deep-Sea Res.* **40**, 115–134.

Maslin, M. A., Shackleton, N. J. and Pflaumann, U. 1995. Surface water temperature, salinity, and density changes in the northeast Atlantic during the last 45,000 years: Heinrich events, deep water formation, and climatic rebounds. *Paleoceanography* **10**, 527–544.

Matear, R. J. and Holloway, G. 1995. Modeling the inorganic phosphorus cycle of the North Pacific using an adjoint data assimilation model to assess the role of dissolved organic phosphorus. *Global Biogeochem. Cycles* **9**, 101–119.

Millero, F. J. 1979. The thermodynamics of the carbonate system in seawater. *Geochim. Cosmochim. Acta* **43**, 1651–1661.

Millero, F. J. 1995. Thermodynamics of the carbon dioxide system in the oceans. *Geochim. Cosmochim. Acta* **59**, 661–677.

Milliman, J. D. 1993. Production and accumulation of calcium carbonate in the ocean: budget of a non-steady state. *Global. Biogeochem. Cycles* **7**, 927–957.

Mook, W. G. 1986. ^{13}C in atmospheric CO_2. *Netherlands J. Sea. Res.* **20**, 211–223.

Murray, J. W., Barber, R. T., Roman, M. R., Bacon, M. P. and Feely, R. A. 1994. Physical and biological controls on carbon cycling in the Equatorial Pacific. *Science* **266**, 58–65.

Najjar, R. G., Sarmiento, J. L. and Toggweiler, J. R. 1992. Downward transport and fate of organic matter in the ocean: Simulations with a general circulation model. *Global Biogeochem. Cycles* **6**, 45–76.

Najjar, R. G. and Toggweiler, J. R. 1993. Reply to the comment by Jackson. *Limnol. Oceanogr.* **38**, 1331–1332.

Nalewajko, C. and Lean, D. R. S. 1980. Phosphorus. In: *The physiological ecology of phytoplankton*, edited by Morris. I. pp. 235–258. University of California Press.

Neftel, A., Oeschger, H., Staffelback, T. and Stauffer, B. 1988. CO_2 record in the Byrd ice core 50,000–5,000 years BP. *Nature* **331**, 609–611.

Oppo, D. W. and Lehman, S. J. 1995. Suborbital timescale variability of North Atlantic Deep Water during the past 200,000 years. *Paleoceanography* **10**, 901–910.

Rasmussen, T. L., Thomsen, E., van Weering, T. C. E. and Labeyrie, L. 1996. Rapid changes in surface and deep water formations at the Faeroe Margin during the last 58,000 years. *Paleoceanography* **11**, 757–771.

Rau, G. H., Takahashi, T., Des Marais, D. J., Repeta, D. J. and Martin, J. H. 1992. The relationship between $\delta^{13}C$ of organic matter and $[CO_2(aq)]$ in ocean surface water: data from a JGOFS site in the northeast Atlantic ocean and a model. *Geochim. Cosmochim. Acta* **56**, 1413–1419.

Rau, G. H., Takahashi, T. and Marais, D. J. D. 1989. Latitudinal variations in plankton $\delta^{13}C$: Implications for CO_2 and productivity in past oceans. *Nature* **341**, 516–518.

Santschi, P. H., Guo, L., Baskaran, M., Trumbore, S., Southon, J., Bianchi, T. S., Honeyman, B. and Cifuentes, L. 1995. Isotopic evidence for the contemporary origin of high-molecular weight organic matter in oceanic environments. *Geochim. Cosmochim. Acta* **59**, 625–631.

Sarmiento, J. L., Murnane, R. and LeQuéré, C. 1995. Air-sea CO_2 transfer and the carbon budget of the North Atlantic. *Phil. Trans. Roy. Soc.* (*Lond.* B) **348**, 211–219.

Schmitz, W. J. 1995. On the interbasin-scale thermohaline circulation. *Rev. Geophys.* **33**, 151–173.

Siegenthaler, U. and Münnich, K. O. 1981. $^{13}C/^{12}C$ fractionation during CO_2 transfer from air to sea. In: *Carbon cycle modelling*, edited by Bolin B. New York. pp. 249–257. John Wiley.

Siegenthaler, U., and Sarmiento, J. L. 1993. Atmospheric carbon dioxide and the ocean. *Nature* **365**, 119–125.

Siegenthaler, U., and Wenk, T. 1984. Rapid atmospheric CO_2 variations and ocean circulation. *Nature* **308**, 624–626.

Skirrow, G. 1975. The dissolved gases: carbon dioxide. In: *Chemical oceanography*, vol. 2, 2nd edition (ed. Riley J. P. and Skirrow G.), pp. 1–181. Academic Press.

Smith, S. 1984. Phosphorus versus nitrogen limitation in the marine environment. *Limnol. Oceanogr.* **29**, 1149–1160.

Smith, S. V. and Hollibaugh, J. T. 1993. Coastal metabolism and the oceanic organic carbon balance. *Rev. Geophys.* **31**, 75–89.

Stocker, T. F., Broecker, W. S. and Wright, D. G. 1994. Carbon uptake experiments with a zonally-averaged global ocean circulation model. *Tellus* **46B**, 103–122.

Stocker, T. F. and Wright, D. G. 1996. Rapid changes in ocean circulation and atmospheric radiocarbon. *Paleoceanography* **11**, 773–796.

Suzuki, Y. 1993. On the measurement of DOC and DON in seawater. *Mar. Chem.* **41**, 287–288.

Tans, P. P., Fung, I. Y. and Takahashi, T. 1990. Observational constraints on the global atmospheric CO_2 budget. *Science* **247**, 1431–1438.

Toggweiler, J. and Samuels. B. 1993. New radiocarbon constraints on the upwelling of abyssal water to the ocean's surface. In: *The global carbon cycle*, edited by M. Heimann. NATO ASI Ser., Ser. I, 15. pp. 333–366.

Toggweiler, J. R., Dixon, K. and Bryan, K. 1989. Simulations of radiocarbon in a coarse-resolution world ocean model, 1, steady state prebomb distributions. *J. Geophys. Res.* **94**, 8217–8242.

Toole, J. M., Polzin, K. L. and Schmitt, R. W. 1994. Estimates of diapycnal mixing in the abyssal ocean. *Science* **264**, 1120–1123.

TTO, 1986. Transient tracers in the ocean: North Atlantic Study: 1 April–19 October 1981. *Shipboard physical and chemical data report*. Physical and Chemical Oceanographic Data Facility. Scripps Institution of Oceanography. Tech. Rep. University of California, San Diego.

Tyrrell, T. and Law, C. 1997. Low nitrate : phosphate ratios in the global ocean. *Nature* **387**, 793–796.

Vidal, L., Labeyrie, L., Cortijo, E., Arnold, M., Duplessy, J.-C., Michel, E., Becqué, S. and Van Weering, T. C. E. 1997. Evidence for changes in the North Atlantic Deep Water linked to meltwater surges during the Heinrich events. *Earth Planet. Sci. Lett.* **146**, 13–27.

Volk, T. and Hoffert. M. I. 1985. Ocean carbon pumps: Analysis of relative strengths and efficiencies in ocean-driven atmospheric CO_2 changes. In: *The carbon cycle and atmospheric CO_2: natural variations archean to present*, edited by Sundquist E. T. and Broecker W. S. Geophys. Monogr. Ser., 32. pp. 99–110. AGU. Washington, D.C.

Weiss, R. F. 1970. The solubility of nitrogen, oxygen and argon in water and seawater. *Deep-Sea Res.* **17**, 721–735.

Williams, P. M. and Druffel, E. R. M. 1987. Radiocarbons in dissolved organic matter in the central North Pacific Ocean. *Nature* **330**, 246–248.

Wright, D. G. 1996. An equation of state for use in ocean models: Eckart's formula revisited. *J. Atm. Oceanic Technolog.* **14**, 735–740.

Wright, D. G. and Stocker, T. F. 1992. Sensitivities of a zonally averaged global ocean circulation model. *J. Geophys. Res.* **97**, 12 707–12 730.

Wright, D. G., Vreugdenhil, C. B. and Hughes, T. M. 1995. Vorticity dynamics and zonally averaged ocean circulation models. *J. Phys. Oceanogr.* **25**, 2141–2154.

Yamanaka, Y. and Tajika, E. 1996. The rôle of the vertical fluxes of particulate organic matter and calcite in the oceanic carbon cycle: Studies using an ocean biogeochemical general circulation model. *Global Biogeochem. Cycles* **10**, 361–382.

Yamanaka, Y. and Tajika, E. 1997. Rôle of dissolved organic matter in the marine biogeochemical cycle. Studies using an ocean biogeochemical general circulation model. *Global Biogeochem. Cycles* **11**, 599–612.

Zhang, J., Quay, P. D. and Wilbur, D. O. 1995. Carbon isotope fractionation during gas-water exchange and dissolution of CO_2. *Geochim. Cosmochim. Acta* **59**, 107–114.